


Species -Shared and -Unique Gyrus Peaks on Human and Macaque Brains

Songyao Zhang, Tuo Zhang , Guannan Cao, Jingchao Zhou, Zhibin He, Xiao Li, Yudan Ren, Tao Liu, Xi Jiang, Lei Guo, Junwei Han, Tianming Liu

School of Automation, Northwestern Polytechnical University, Xi'an, China • College of Science, North China University of Science and Technology, Tangshan, China • School of Information Technology, Northwest University, Xi'an, China • School of Life Science and Technology, MOE Key Lab for Neuroinformation, University of Electronic Science and Technology of China, Chengdu, China • Cortical Architecture Imaging and Discovery Lab, Department of Computer Science and Bioimaging Research Center, University of Georgia, Athens, GA, USA

Reviewed Preprint

Revised by authors after peer review.

About eLife's process

Reviewed preprint version 2

March 21, 2024 (this version)

Reviewed preprint version 1

November 22, 2023

Posted to preprint server

July 29, 2023

Sent for peer review

July 11, 2023

 https://en.wikipedia.org/wiki/Open_access

 Copyright information

Abstract

Cortical folding is an important feature of primate brains that plays a crucial role in various cognitive and behavioral processes. Extensive research has revealed both similarities and differences in folding morphology and brain function among primates including macaque and human. The folding morphology is the basis of brain function, making cross-species studies on folding morphology important for understanding brain function and species evolution. However, prior studies on cross-species folding morphology mainly focused on partial regions of the cortex instead of the entire brain. Previously, we defined a whole-brain landmark based on folding morphology: the gyrus peak. It was found to exist stably across individuals and ages in both human and macaque brains. In this study, we identified shared and unique gyrus peaks in human and macaque, and investigated the similarities and differences in the spatial distribution, anatomical morphology, and functional connectivity of them.

eLife assessment

This **important** paper compares cross-species cortical folding patterns in human and non-human primates, showing that most gyrus peaks shared across species are in lower-order cortical regions. The supporting evidence is **solid** and multi-faceted, encompassing anatomy, connectivity and gene expression. This paper will be of interest to a broad readership within the neuroscience community, especially for those interested in cross-species correspondences in brain organisation.

Introduction

Humans and macaques share a common ancestor, but they have diverged evolutionarily approximately 25 million years ago ([Hill et al. \(2010\)](#)). As a result of genetic changes, environmental factors, and selective pressures ([Lecouvet et al. \(1997\)](#)), they have developed distinct brain structures and functions. Cortical folds are important features of primate brains.

The primary driver of cortical folding is the differential growth between cortical and subcortical layers. During the gyrification process in the cortex, areas with high-density stiff axonal fiber bundles towards gyri. The brain's folding pattern formed through a series of complex processes. The folding patterns in the brain, formed through a series of complex processes, are found to play a crucial role in various cognitive and behavioral processes, including perception, action, and cognition ([Fornito et al. \(2004\)](#); [Cachia et al. \(2018\)](#); [Yang et al. \(2019\)](#); [Whittle et al. \(2009\)](#)). Studies have revealed differences and similarities in fold morphology and brain function between humans and macaques ([Semendeferi et al. \(2002\)](#)). Furthermore, there is an intricate relationship between the similarities and differences in cortical folding morphology and the similarities and differences in brain function. For example, humans possess a larger prefrontal cortex compared to macaques, which gives them executive functions such as planning, decision-making, and working memory ([Semendeferi et al. \(2002\)](#)). The higher cognitive and affective functions observed in human compared to macaque are also associated with the larger proportion of their association cortex in the cortical surface ([Glasser et al. \(2013\)](#); [Rilling \(2014\)](#); [Rolls and Grabenhorst \(2008\)](#)). The variations in cortical folding morphology, as well as the differences in brain function, may reflect the adaptation of species to diverse cognitive, social, and ecological demands. Despite variations in morphological and functional characteristics of the cortical folds among different species, there are also many commonalities, indicating relative conservation in the evolutionary process ([Van Essen et al. \(2019\)](#)). For example, gyrencephalic primates which share many primary sulci, such as the lateral, superior temporal, and (except for the marmoset) central sulci, exhibit similarities in both morphology and brain function ([White et al. \(1997\)](#); [Ferrier \(1873\)](#); [Friedrich et al. \(2021\)](#)). Additionally, by comparing the brain activity of chimpanzees during tasks with nonsocial tasks and at rest, it was found that the cortical midline areas of chimpanzees deactivate during these tasks. This suggests that the DMN of chimpanzees is anatomically and functionally similar to that of humans ([Barks et al. \(2015\)](#)). Some studies have found that in species including humans and monkeys, strongly interconnected regions are consistently separated by outward folds, whereas weakly connected regions are consistently separated by inward folds. This folding pattern is associated with brain connectivity, suggests a certain similarity in the mechanisms underlying cortical folding in humans and monkeys ([Essen \(1997\)](#); [Sereno et al. \(1995\)](#); [Sousa et al. \(1991\)](#)). In summary, the folding patterns and functional profiles of cortical regions demonstrate both similarities and differences across different species. These similarities may reflect evolutionary conserved functions, while the differences may indicate species-specific features ([de Lange et al. \(2019\)](#); [Buckner and Krienen \(2013\)](#); [Patel et al. \(2015\)](#)).

Most of the current cross-species studies are based on one or several anatomical landmarks ([Eichert et al. \(2019\)](#); [Goulas et al. \(2014\)](#); [Van Essen and Dierker \(2007\)](#); [Van Essen et al. \(2018\)](#)), which cannot really solve the cross-species analysis needs of the whole brain. The definition of a whole-brain anatomical landmark across species is a complex task due to differences in brain size, cortical folding patterns, and the relative size and location of different brain regions. As a landmark defined based on cortical fold pattern, the gyral peak, as the maximum in height on the cortex, has been discovered and studied in both humans and macaques ([Zhang et al. \(2022, 2023\)](#)). It is defined as the local highest point of the gyri. In our previous work, there are many similarities between the findings of humans and macaques regarding gyral peaks. For example, both species were able to detect consistent gyral peaks among individuals on the cerebral cortex. And it was even consistent across ages in the longitudinal macaque dataset ([Zhang et al. \(2022\)](#)). In both of these works there is a discussion of peaks' anatomical feature and inter-individual consistency. In the study of macaques, it has been observed that the peak consistently present across individuals is located on more curved gyri ([Zhang et al. \(2022\)](#)). Similar conclusions have been drawn in human brain research ([Zhang et al. \(2023\)](#)). While some findings are not entirely the same between humans and macaques. For example, the higher consistency peaks in humans possessing smaller structural connectivity properties, while the conclusion is opposite in macaques. In addition, there are some conclusions that have been

verified on only one species. Based on the aforementioned advantages of gyral peaks, they are highly suitable as anatomical landmarks for cross-species research to infer the developmental and evolutionary aspects of cortical folding and brain functionality.

Here, we investigated shared and unique peaks across individuals and species. We first identified the group-wise peak clusters of human and macaque brains, respectively, and aligned the macaque peak clusters onto the human brain surface using cross-species registration methods ([Xu et al. \(2020\)](#)). This allowed us to identify the shared and unique peak clusters between the two species. Then, we compared the inter-individual consistency of shared and unique clusters within each species, and investigated whether there was a relationship between the inter-individual consistency of shared clusters between human and macaque. Additionally, we examined the anatomical features of these shared and unique clusters and calculated the functional and structural connectivity matrices of the human and macaque brains. Then we used Brain Connectivity Toolbox (BCT, [Rubinov and Sporns \(2010\)](#)) to compute the node features of shared and unique clusters. Furthermore, we examined the spatial relationships between these clusters and different brain regions of multiple atlases. Finally, we used human brain RNA-seq data to select important genes from shared and unique peaks in classification tasks. Our study provides a medium based on cortical folding patterns for cross-species cortical analysis. Through such a medium, we can explore the derivation and specialization of human and macaque brain and understand the rules of how the brain is constructed during development and evolution ([Krubitzer \(2007\)](#)).

Results

Locations of Shared and Unique Peak Clusters

To obtain shared and unique gyral peaks between species, we first extracted peak clusters for each species. The definition of peaks and the method for extracting peak clusters within each species are described in the Materials and Methods section. Then, we employed a cross-species registration method ([Xu et al. \(2020\)](#)) to align the macaque peak clusters onto the human brain surface. **Figure. 1** (a) top and middle panels display the locations of all peak clusters found in both human and macaque brains (Human: LH-96, RH-96; Macaque: LH-42, RH-43). Then we use the cross-species registration method ([Xu et al. \(2020\)](#)) to register the peak clusters of the macaque brain onto the human brain surface (**Figure. 1** (a) bottom panel uses the same color-coding as the macaque surface to represent the same cluster). Next, based on the definition of shared peak clusters (see Materials and Methods), we identified shared and unique gyral peaks between the two species. **Figure. 1** (b) shows the locations of shared peak clusters between the two species, with 25 shared peaks in the left hemisphere while 26 in the right (the locations of all human shared peaks are reported in [Table A4](#)). For the purpose of comparison, the shared gyral peak clusters of two species were displayed on the surface of the human brain template (Conte69, [Van Essen et al. \(2012b\)](#)) with the same color coding for corresponding peak clusters on the two species. The results of shared peak clusters on the macaque surface template are placed in Supplementary Information. **Figure. 1** (c) shows the locations of unique peak clusters found in each species, with 141 (LH-71, RH-70) unique peak clusters found in the human brain and 34 (LH-17, RH-17) found in the macaque brain. The unique peaks found in the human brain were mapped onto the Conte69, while those found in the macaque brain were mapped onto the Yerkes19 ([Van Essen et al. \(2012a\)](#)) template surface. It is worth noting that for each species, the union of the clusters in **Figure. 1** (b) and **Figure. 1** (c) is the same as the clusters in **Figure. 1** (a) (including color).

To investigate the regions where shared and unique peaks are located, we utilized the ColeAnticevic Brain-wide Network Partition (CA network, [Ji et al. \(2019\)](#)), which includes in total 12 functional networks (**Figure. 2** (a) right panel) based on the MMP (multimodal parcellation,



Figure 1.

(a) Top: 192 gyral peak clusters of human on human brain template (Conte69, [Van Essen et al. \(2012b\)](#)). Middle: 85 gyral peak clusters of macaque on macaque brain template (Yerkes19, [Van Essen et al. \(2012a\)](#)). Bottom: The results of mapping macaque gyral peak clusters on the human brain template by the cross-species registration ([Xu et al. \(2020\)](#)). The same color of middle and bottom surface indicates the corresponding peak clusters. (b) Peak clusters shared by human and macaque (LH-25, RH-26). On the same hemisphere of the brain, the corresponding-colored regions on both human and macaque represent the corresponding shared peak clusters. In addition, the color of the left and right hemisphere clusters are not related. (c) Unique peak clusters of two species map on the surface of their respective surface template.

[Glasser et al. \(2016\)](#)). We then projected the human Cole-Anticevic network on the macaque surface using [Xu et al. \(2020\)](#) to qualitatively compare the differences in the distribution of cluster centers between human and macaque. It is important to emphasize that while the shared peak clusters were obtained through cross-species registration, and the human brain network (Cole-Anticevic) was also transferred to the macaque surface using cross-species registration, it is still meaningful to compare the distribution of shared peak centers between humans and macaques. This is because the intersection of clusters (one of the definition of shared peak clusters) does not necessarily imply that the centers of peak clusters are located in the same brain region.

We counted the number of shared and unique peaks distributed in different brain networks (**Figure. 2** (a)). In human brain, most shared peak cluster centers are distributed in the networks such as somatomotor (SMN), visual 1 (V1), and visual 2 (V2), while most human unique peak cluster centers are located in the networks such as default-mode network (DMN), cingulo-opercular (CON), and frontoparietal (FPN). In the macaque brain, shared peak cluster centers most distributed in the V2, DMN, and CON, while unique peak cluster centers most distributed in the higher-order networks such as DMN, language (Lan), and dorsal attention (DAN). In order to eliminate the influence of different brain area sizes on the count of peak cluster, we normalized the count by the regional surface area and reported in **Figure. A2**.

In general, to clarify the distribution of shared and unique peaks in the high-order and low-order networks, we divided 12 brain networks in Cole-Anticevic atlas into the low-order networks (visual 1 (V1), visual 2 (V2), auditory (Aud), somatomotor (SMN), posterior multimodal (PMN), ventral multimodal (VMN), and orbito-affective networks (OAN)) and higher-order networks (include cingulo-opercular (CON), dorsal attention (DAN), language (Lan), frontoparietal (FPN), default mode network (DMN)) based on previous research ([Golesorkhi et al. \(2022\)](#); [Ito et al. \(2020\)](#)). On this lower/higher-order division, we reported the number of shared and unique peaks in both species in **Table 1**. **Figure. 2** (a) and Table.1 collectively indicate a conclusion: whether in humans or macaques, shared peaks are more distributed in lower-order networks, while unique peaks are more in higher-order networks. This observation is particularly pronounced in humans.

While it is known where shared and unique peaks are distributed across different brain networks, the dominance of each type of peak within each networks remains unrevealed. **Figure. 2** (b) reports the ratio between peak count and unique peak count for each network, such that the networks where the most shared or unique peaks are found can be easily highlighted. To mitigate potential imbalances in proportions caused by differences in the absolute numbers of each category (shared or unique) of peak, the proportions of peaks within their respective categories were utilized in the calculations. The pink and green color bins represent ratios of shared and unique peaks, respectively. The dark blue dashed line represents the 50% reference line. In general, from left to right in the figure, the ratio of shared peaks decreases gradually while the ratio of unique peaks increases, suggesting that shared peaks are more (>0.5, above the dashed line) on lower-order networks (orange font), while unique peaks are generally more on higher-order networks (blue font). In specific, in human brains, the brain networks with a higher abundance of shared peaks are Aud, VMN, V1, SMN, and V2; whereas in macaques, they are CON, VMN, V1, V2, FPN, and SMN. Again, in the human brains, the disparity between shared and unique peaks tends to be more significant (further away from the reference line), for both lower-order and higher-order networks, respectively. In contrast, in the macaque brains, the disparity between shared and unique peaks is less significant (closer to the reference line). The ratio of shared and unique peaks is around 0.5 for 6 out of all 10 networks (including both lower and higher-order ones).

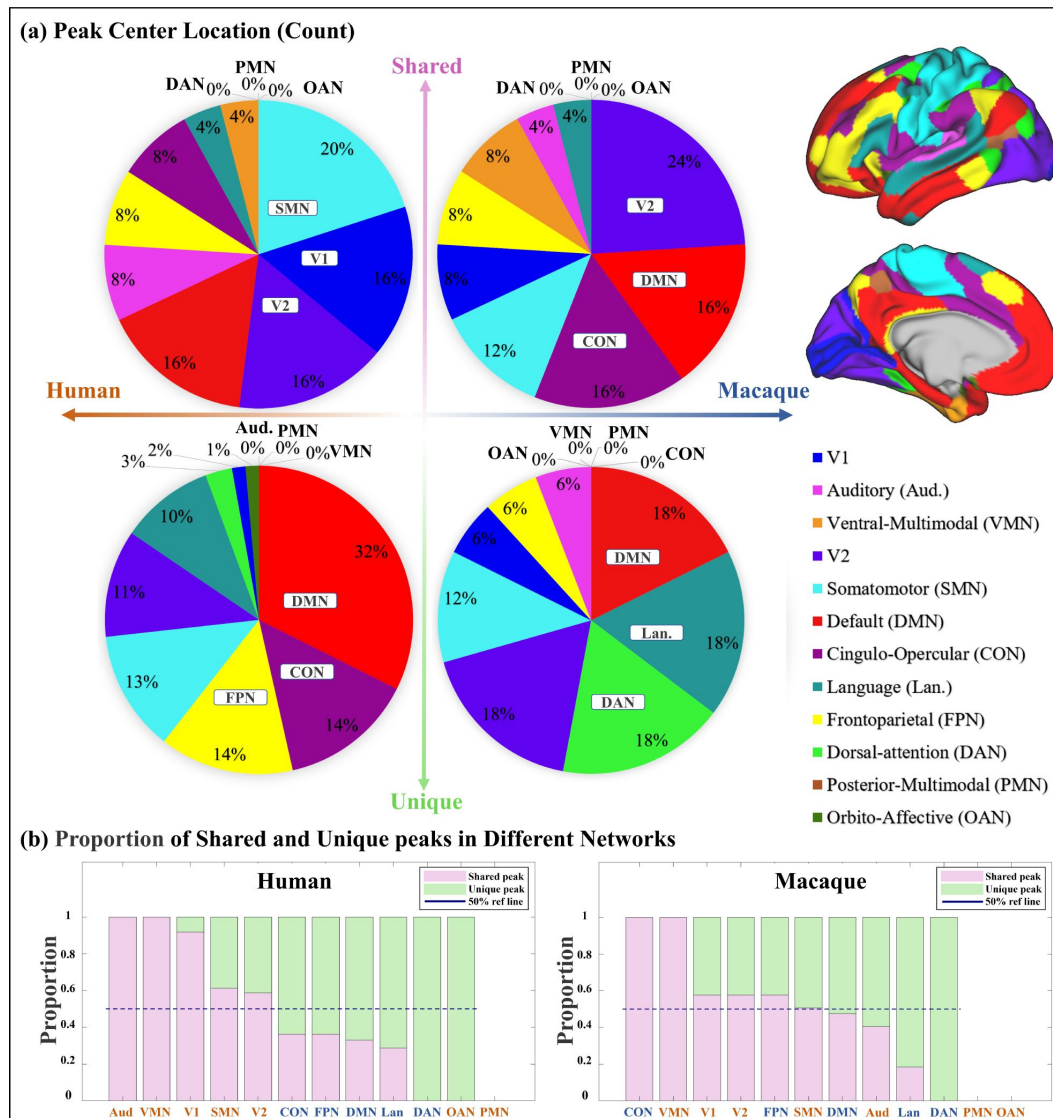


Figure 2.

(a) Pie chart shows the count of shared and unique peaks across different brain networks for both human and macaque. Right panel shows the Cole-Anticevic (CA) networks ([Ji et al. \(2019\)](#)) on human surface as a reference. (b) The ratio of shared and unique peaks in each brain network in the Cole-Anticevic (CA) atlas. The pink and green color bins represent ratios of shared and unique peaks, respectively. The dark blue dashed line represents the 50% reference line. For each brain region, the sum of the ratios of shared and unique peaks is equal to 1.

Lower/Higher cortex	Human	Macaque
Shared peak	33/18	29/22
Unique peak	37/104	14/20

Table 1.

The number of shared and unique peaks in lower- and higher-order brain networks of the two species. Lower-order networks include visual 1 (V1), visual 2 (V2), auditory (Aud), somatomotor (SMN), posterior multimodal (PMN), ventral multimodal (VMN), and orbito-affective networks (OAN), higher-order networks include cingulo-opercular (CON), dorsal attention (DAN), language (Lan), frontoparietal (FPN), default-mode network (DMN).

Consistency of Unique/Shared Peak Clusters

In our previous researches, the inter-individual consistency of peaks is a measure to assess whether peaks exist consistently in different individuals ([Zhang et al. \(2022, 2023\)](#)). To explore the inter-individual consistency of shared and unique peak clusters in macaques and humans, we calculated the mean count covered by these clusters and normalized by the number of individuals, as presented in [Figure. 3](#) (a). In both human and macaque, the consistency of shared peak clusters is significantly greater than that of unique peak clusters ($p < 0.001$, t -value=4.74 for human and 2.67 for macaque). Additionally, the overall consistency of peaks in the macaque brain is much higher than that in the human brain, indicating that the peaks in the different macaque brain are more concentrated in spatial distribution. Furthermore, we performed linear regression analysis on the average counts of all corresponding shared peak clusters of human and macaque. The horizontal and vertical axes of the [Figure. 3](#) (b) represent the average count of shared peaks in the macaque and human brains, respectively. The Pearson correlation coefficient (PCC) of the inter-species consistency of the left and right brain is 0.20 and 0.26 ($p > 0.05$ for all), respectively. The result of linear regression shows that there is a positive correlation in the inter-individual consistency of shared peaks between macaque and human brains, but it is not statistically significant (with R^2 for the left and right brain are 0.07 and 0.01, respectively).

Anatomical Features of Shared and Unique Peaks

We then calculated the mean of the anatomical features of shared and unique peaks on all individuals of both species. The shared and unique peaks in each individual were obtained by calculating the intersection between the group-wise shared and unique clusters and the gyral peaks in each individual. We found that, whether in human or macaque, the sulcs and local surface area of shared peaks are larger than those of the unique peaks, but the curvatures are smaller. Due to issues with MRI data quality and technical limitations, we only reconstructed the white matter surface of the macaque brain and did not have the gray matter surface available. Therefore, it was not possible to calculate cortical thickness for the macaque dataset. Additionally, due to the unavailability of T2 data in the macaque dataset, the myelin feature was also missing. For the exclusive anatomical features of human, shared gyral peaks are located in cortical regions with thinner cortex but larger myelin in contrast of unique peaks ([Table 2](#)). Our statistical analysis using t-tests demonstrated that the p-value for shared and unique peaks of all features is less than 0.001 except local surface area of macaque.

Functional Connectivity Characteristics of Shared and Unique Peaks

[Table 3](#) shows the mean (\pm SD) of node properties of the functional connectivity for all shared and unique peak clusters in human and macaque, including degree, strength, clustering coefficient (CC), betweenness, and efficiency. In general, our results demonstrate that shared peaks exhibit significantly ($p < 0.001$) larger degree, strength, clustering coefficient, betweenness, and efficiency values than unique peaks (except for betweenness and efficiency of macaque) for the functional connectivity characteristics. The mean values of all node properties, as well as the p-values and t-values of the t-test between shared and unique peaks, are all displayed in [Table 3](#). In addition, we also make a comparison between shared and unique peaks on the structural connectivity matrix of human brain, and the results are presented in [Table A5](#) of the Supplementary Information (due to the poor tracking effect of dti fiber tractography in the macaque data, we only calculated the structural connection matrix of human brain).

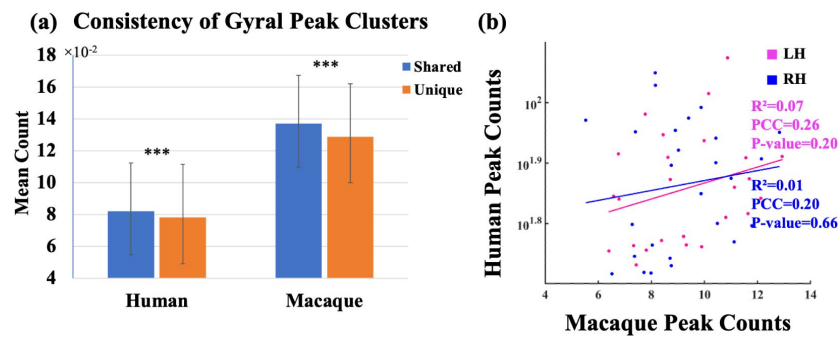


Figure 3.

(a) Mean peak count (\pm SD) covered by shared and unique peak clusters in two species. ***indicates $p < 0.001$. The t-values for the t-tests in humans and macaques are 4.74 and 2.67, respectively. (b) Linear regression results of the consistency of peak clusters shared between macaque and human brains. The pink and blue colors represent the left and right hemispheres, respectively. The results of the linear regression are depicted in the figure. While there was a positive correlation observed in the consistency of gyral peaks between macaque and human, the obtained p-value for the fitted results exceeded the significance threshold of 0.05.

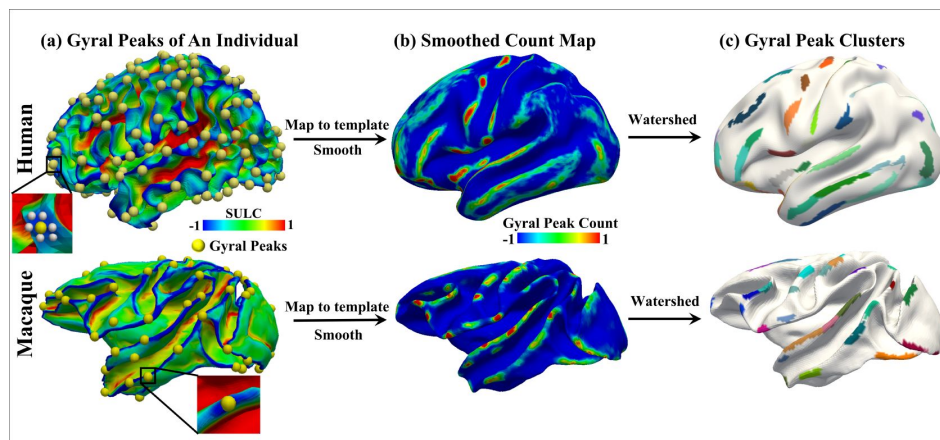


Figure 4.

Peak cluster extraction pipeline. The two rows represent the human brain and the macaque brain, respectively. (a) shows the locations of all extracted peaks in an individual. (b) Due to resampling of the human and macaque surface, there is a vertex-to-vertex correspondence between individuals. Therefore, all individual peaks were placed on the template brain surface and undergo isotropic smoothing, resulting in the count map shown in (b), where the highlighted regions indicate a higher frequency of peak occurrences across individuals. (c) shows the results of clustering the count map using watershed algorithm, resulting in peak clusters for both species. A total of 192 peak clusters were detected in the human brain, while 85 peak clusters were detected in the macaque brain.

	Human					Macaque		
	Sulc	Curv	Myelin	Thickness	Area	Sulc	Curv	Area
Shared	0.93±0.05	0.31±0.02	1.85±0.10	2.71±0.14	1.19±0.09	0.86±0.03	0.55±0.03	0.94±0.44
Unique	0.79±0.05	0.32±0.01	1.83±0.11	2.94±0.12	1.09±0.05	0.80±0.04	0.58±0.03	0.91±0.17
p	<0.001	<0.001	<0.001	<0.001	<0.001	<0.001	<0.001	0.59
t	58.43	-16.26	6.51	-36.67	30.43	6.07	-5.32	0.54

Table 2.

The mean (\pm SD) of anatomical features, as well as the p-values and t-values of the t-test between shared and unique peak clusters. In the t-test, n for human is 880 and for macaque is 591. The bold font is the one with the larger values of shared and unique peaks.

		Degree	Strength	CC	Betweenness	Efficiency
Human FC	Shared	141.13±30.46	52.27±22.84	0.20±0.07	1.87±0.74($\times 10^3$)	0.25±0.07
	Unique	119.88±18.03	44.35±15.24	0.19±0.05	1.46±0.43($\times 10^3$)	0.24±0.06
	p	<0.001	<0.001	<0.001	<0.001	<0.001
	t	7.78	5.24	3.94	4.42	3.37
Macaque FC	Shared	136.60±21.89	43.74±8.85	0.18±0.05	2.00±0.50($\times 10^3$)	0.25±0.07
	Unique	134.69±23.51	43.30±8.15	0.17±0.05	2.18±0.60($\times 10^3$)	0.24±0.07
	p	<0.01	<0.001	<0.01	<0.001	>0.05
	t	2.98	5.01	2.64	-6.52	0.53

Table 3.

The mean (\pm SD) functional connectivity characteristics, as well as the p-values and t-values of the t-test between shared and unique peak clusters of human and macaque. In the t-test, n for human is 880 and for macaque is 591. The bold font represent the larger values between the shared peak and unique peaks.

Spatial Relationship Between Peaks and Functional Regions

To assess the relative spatial relationship between the two types of peaks and different brain regions, we calculated the number of brain regions where each type of peak appeared within a 3-ring neighborhood. We utilized various types of brain atlases, including those based on functional, structural, and cytoarchitectural. These atlases are crucial because they contain diverse features of the brain, helping to identify spatial patterns of shared and unique peaks across multiple references. **Table 4** and **Table 5** present the results for 10 human brain atlases and 3 macaque brain atlases, respectively (results of all other human atlases are presented in **Table A6**). We utilized false discovery rate (FDR) correction for multiple comparisons, and the corrected p-values are reported in tables (n=880 for human and n=591 for macaque). The observation that more diverse brain regions around shared peaks than around unique peaks for multiple brain atlases with a median parcellation resolution (7 parcels to 300 parcels), demonstrating the robustness of the conclusion.

Gene Analysis of Shared and Unique Peak Clusters Based on Lasso

Finally, to study whether there are significant differences in gene expression between the two types of peaks, we utilized the surface-based gene expression dataset Allen Human Brain Atlas (AHBA) ((*Arnatkevičiūtė et al. (2019)*), (*Hawrylycz et al. (2012)*))) and employed the widely used lasso method for gene selection. The preprocessed AHBA gene data is in the form of region×gene and the region above referred to the parcellation of a certain atlas, such as Aparc, Schaefer100, Schaefer500, Schaefer1000, etc. We finally selected Schaefer500 atlas for this study because high resolution may result in some areas with no gene data (more details refer to *Arnatkevičiūtė et al. (2019)*), while low resolution may result in multiple categories of clusters being located in the same region. Therefore, Schaefer500 was chosen as the most suitable atlas for our analysis. Before using lasso for feature selection, the determination of the Lambda parameter is necessary to regulate the number of selected features. For parameter selection, we employed 10-fold cross validation for parameter selection. By considering the maximization of accuracy (acc) and minimization of mean squared error (MSE) simultaneously, the lambda value was ultimately determined to be 0.027 (**Figure. 5** (b)). The accuracy of training set was 0.84, and the MSE was 0.64; The accuracy of test set was 0.75, and the MSE was 1.00. Finally, we utilized the Lasso method to select 28 genes with significant impacts on the classification of shared and unique peaks. Then we performed Welch's t-tests to compare the expression of the 28 genes in the shared and unique peak clusters. The gene list and the corresponding Welch's t-tests results were shown in **Table A7**. Ultimately, seven genes showed significant differential expression between shared and unique peaks. These genes were PECAM1, TLR1, SNAP29, DHRS4, BHMT2, PLBD1, KCNH5. Brief descriptions of their functions are listed in **Table 6**. All gene functions descriptions were derived from the NCBI website (<https://www.ncbi.nlm.nih.gov/>).

Discussion and Conclusion

In this study, 192 gyral peaks were detected in the human brain, and 85 gyral peaks were detected in the macaque brain. Additionally, 51 pairs of shared peaks (25 in the left and 26 in the right hemisphere) were identified using cross-species registration, as previously reported by (*Xu et al. (2020)*). The following findings were observed:

1. Spatial distribution: Whether in humans or macaques, shared peaks are more predominantly distributed in lower-order networks, while unique peaks are more prevalent in higher-order networks. This conclusion is particularly pronounced in humans.

Atlas Name	Glasser2016	Schaefer-100	Schaefer-200	Schaefer-300	Vosdewael-100
Share Nbr	2.43±0.15	1.89±0.12	2.12±0.11	2.23±0.11	1.57±0.17
Unique Nbr	2.37±0.09	1.74±0.09	2.08±0.10	2.17±0.10	1.46±0.10
p	<0.001	<0.001	<0.001	<0.001	<0.001
t	8.32	26.66	4.50	18.08	34.09
Atlas Name	Yeo2011(17)	Aparc	Aparc2009	BA	Cole-Anticevic
Share Nbr	1.76±0.11	1.58±0.12	1.95±0.13	1.58±0.12	1.65±0.11
Unique Nbr	1.73±0.08	1.33±0.07	1.94±0.09	1.29±0.08	1.57±0.07
p	<0.001	<0.001	<0.001	<0.001	<0.001
t	22.29	56.37	3.80	69.84	22.44

Table 4.

The mean values (\pm SD) of brain regions that appeared within a 3-ring neighborhood for shared and unique peaks in 10 common human atlases. All the shared peaks in the table have a greater number of neighboring brain regions compared to the unique peaks. All $p < 0.001$, false discovery rate (FDR) corrected.

Atlas Name	Markov91	Cole-Anticevic	BA05
Share Nbr	2.73±0.27	1.77±0.17	1.61±0.16
Unique Nbr	2.16±0.15	1.58±0.16	1.80±0.16
p	<0.001	<0.001	<0.001
t	-7.4	14.93	6.49

Table 5.

The mean values (\pm SD) of brain regions that appeared within a 3-ring neighborhood for shared and unique peaks in 3 common macaque atlases. For both Markov91 and Cole-Anticevic atlas, the shared peaks has more variety of functional regions around it than the unique peaks. But for the atlas BA05, the conclusion was reversed. The bold font represent the larger values between the shared peak and unique peaks. All $p < 0.001$, false discovery rate (FDR) corrected.

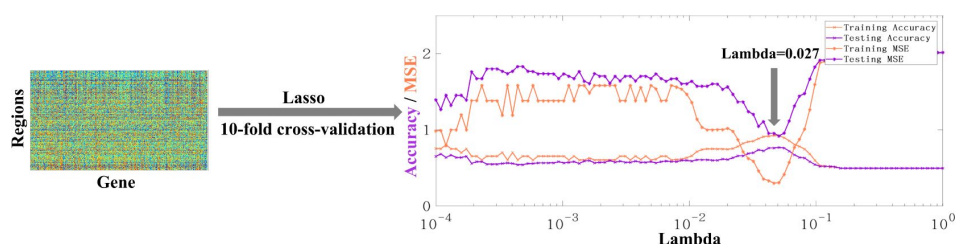


Figure 5.

The original form of AHBA data is region \times gene. The accuracy and MSE line charts of the training set and testing set corresponding to lambda from 10^{-4} to 1. Purple and orange respectively represent the accuracy and mse obtained by 10-fold cross verification. The final lambda determined is 0.027, which can ensure the maximum accuracy and minimum MSE at the same time.

Gene Symbol	Gene Function
PECAM1	The protein encoded by this gene is found on the surface of platelets, monocytes, neutrophils, and some types of T-cells, and makes up a large portion of endothelial cell intercellular junctions. The encoded protein is a member of the immunoglobulin superfamily and is likely involved in leukocyte migration, angiogenesis, and integrin activation. [provided by RefSeq, May 2010]
TLR1	The protein encoded by this gene is a member of the Toll-like receptor (TLR) family which plays a fundamental role in pathogen recognition and activation of innate immunity. They recognize pathogen-associated molecular patterns (PAMPs) that are expressed on infectious agents, and mediate the production of cytokines necessary for the development of effective immunity. [provided by RefSeq, Jul 2008]
SNAP29	This gene, belonging to the SNAP25 gene family, encodes a protein involved in various membrane trafficking processes. Other members of this gene family, such as SNAP23 and SNAP25, encode proteins that bind to a syntaxin protein and facilitate the docking and fusion of synaptic vesicle membranes with the plasma membrane. [provided by RefSeq, Jul 2008]
DHRS4	Exhibits protein binding and oxidoreductase activities, involved in cellular metabolic processes including ketone metabolism, regulation of reactive oxygen species, and steroid metabolism. Found in the nucleus and peroxisomal membrane. [provided by Alliance of Genome Resources, Apr 2022]
BHMT2	Homocysteine, a sulfur-containing amino acid, is crucial for methylation reactions. The protein encoded by this gene is one of two methyltransferases that facilitate the transfer of a methyl group from betaine to homocysteine. Irregularities in homocysteine metabolism have been linked to conditions ranging from vascular disease to neural tube birth defects. This gene has alternatively spliced transcript variants encoding different isoforms.[provided by RefSeq, May 2010]
PLBD1	Predicted to enable phospholipase activity. Predicted to be involved in phospholipid catabolic process. Located in extracellular space. [provided by Alliance of Genome Resources, Apr 2022]
KCNH5	This gene encodes a member of voltage-gated potassium channels. Members of this family have diverse functions, including regulating neurotransmitter and hormone release, cardiac function, and cell volume. This protein is an outward-rectifying, noninactivating channel. Alternative splicing results in multiple transcript variants. [provided by RefSeq, Jul 2013]

Table 6.

Seven genes were selected using LASSO that showed significant differential expression in shared and unique peaks.

2. Consistency: The inter-individual consistency of shared peaks within each species was greater than that of unique peaks. The consistency of shared peaks in the human and macaque brains exhibits a positive correlation (not-significant though).
3. Anatomy: In both human and macaque, it can be found that the sulcs and local surface area of shared peaks are larger but the curvatures are smaller compared to unique peaks in each species. Furthermore, for the exclusive anatomical features of human, shared gyral peaks are located in cortical regions with thinner cortex but larger myelin in contrast of unique peaks.
4. Brain connectivity: Shared peaks in the structural (human only) and functional (human and macaque) graph metrics exhibited higher values for degree, strength, clustering coefficient, betweenness and efficiency compared to unique peaks in both species (except for betweenness and efficiency of the macaque).
5. Relationship with brain regions: Across multiple brain atlases in both species, shared peaks, compared to unique peaks, were found in clusters encompassed by a more diverse array of brain regions.
6. Gene analysis: Using Lasso to perform feature selection on all genes, we found some genes related to brain function played an important role in the classification of shared and unique peaks.

We observed that whether in humans or macaques, shared peaks are more distributed in lower-order networks, while unique peaks are more in higher-order networks (**Figure. 2** and **Table 1**). This observation is particularly pronounced in humans. This finding is in line with previous conclusions that cortical regions associated with motor and sensory functions are relatively conserved across species ([Hopkins et al. \(2014\)](#); [Krubitzer \(2007\)](#); [Xu et al. \(2020\)](#); [Teissier and Pierani \(2021\)](#)), while the unique peaks on human appear in brain regions that are specific to human, such as language areas. One possible explanation is the disproportionate expansion of multiple, distributed regions of association cortex relative to sensory regions during species evolution ([Krubitzer \(2007\)](#); [Buckner and Krienen \(2013\)](#)). The expansion of these regions, which untethered them from the constraints of sensory hierarchies and established species-specific functional associations, is the foundation of the ‘tethering hypothesis’ ([Buckner et al. \(2013\)](#)). Evolutionary psychology and neuroscience indicate that this differential regional allometric growth arises from developmental constraints and represents an adaptive adjustment by the brain to optimize its functional organization ([Montgomery \(2013\)](#); [Montgomery et al. \(2016\)](#); [Willemet \(2015\)](#)). Based on these studies, interspecies conservation of sensorimotor regions and uniqueness of higher-order brain regions are easily understood, and our study provides additional supports to this viewpoint by examining cortical folding.

In each pie chart of **Figure. 2** (a), we specifically highlighted the top three ranked brain networks in both species. Although the pie chart also generally supports the above results, two brain networks deserve further discussion, as shown in **Figure. 2** (a). They are DMN and CON, two higher-order networks where shared peaks are higher count rank among shared peak occupied networks (the second-ranked and the third-ranked on macaque shared peaks; the fourth-ranked and the fifth-ranked on human shared peaks). The cingulo-opercular network (CON) is a brain network associated with action, goal, arousal, and pain. However, a study found that three newly discovered areas of the primary motor cortex that exhibit strong functional connectivity with the CON region, forming a novel network known as the somato-cognitive action network (SCAN) ([Gordon et al. \(2023\)](#)). The SCAN integrates body control (motor and autonomic) and action planning, consistent with the idea that aspects of higher-level executive control might derive from movement coordination ([Llinás \(2002\)](#); [Gordon et al. \(2023\)](#)). CON may be shared in the form of the SCAN network across these two species. This could explain in part the results in **Figure. 2** (a) that shared peaks are more on CONs. Default-mode network (DMN) is an ensemble of brain regions that are active in passive tasks, includes the anterior and posterior cingulate cortex, medial and lateral parietal cortex, and medial prefrontal cortex ([Buckner et al. \(2008\)](#)). Although DMN is considered a higher-order brain network, numerous studies have provided

evidence of its homologous presence in both humans and macaques. Many existing studies have confirmed the similarity between the DMN regions in humans and macaques from various perspectives, including cytoarchitectonic ([Parvizi et al. \(2006\)](#); [Buckner et al. \(2008\)](#); [Caminiti et al. \(2010\)](#)) and anatomical tracing ([Vincent et al. \(2007\)](#)). These studies all support the notion that some elements of the DMN may be conserved across primate species ([Mantini et al. \(2011\)](#)). In general, the partial sharing of DMN between humans and macaques may be attributed to the higher occurrence of shared peaks within the DMN.

The consistency of peaks across individuals is an important indicator. It reflects the similarity in cortical folding morphology among individuals. When we compared the consistency of shared and unique peaks, we discovered that shared peaks exhibit greater stability within the same species across different individuals. This observation was as we expected because the similarities in folding patterns could be related to preferences for neurons to migrate in cortical areas ([Kriegstein et al. \(2006\)](#); [Friedrich et al. \(2021\)](#)) and genetically coded ([Friedrich et al. \(2021\)](#)). These genes, which regulate the cortical structural morphology, are likely conserved in both human and macaque brains over time. Therefore, this has led to the stable presence of cortical folding patterns in both human and macaque species. Moreover, we found that the overall consistency of peaks in the macaque brain is much higher than that in the human brain, indicating that the spatial distribution of gyral peaks in the macaque brain is more concentrated across individuals compared to humans. This is possibly due to the simpler folding patterns that are more easily retained between individuals in macaque and human brains. Next, we computed the correlation between shared peaks consistency across species and found a positive correlation (not-significant though) between the consistency of human and macaque (**Figure. 3**). This implies that peaks that are widespread in the human brain are also widespread in corresponding regions in the macaque brain. These findings further supports the homology of human and macaque brain structures ([Sereno and Tootell \(2005\)](#); [Modha and Singh \(2010\)](#)).

The spatial distribution of shared/unique gyral peaks across species, as defined by our study, is not random but shows discernable patterns, which can be verified through statistical analysis of anatomical features (**Table 2**). The shared peaks, in comparison to the unique peaks, exhibit larger sulc and local surface area, but smaller curvature. Furthermore, in human-specific anatomical features (not available in the macaque dataset), the shared gyral peaks exhibit thinner cortex and greater myelination. The associations among these anatomical features can validate the regularity of the distribution of shared and unique peaks. The associations among these anatomical properties of the brain have been extensively verified in previous studies, including the strong positive correlation between sulc and local surface area ([Yang et al. \(2016\)](#)), the negative correlation between myelin and curvature in most regions ([Schmitt et al. \(2021\)](#)), and the negative correlation between local surface area and cortical thickness ([Maingault et al. \(2016\)](#)). These findings confirm the validity of the anatomical characteristics of shared peaks and unique peaks. While many studies have confirmed the positive correlation of sulc and curvature throughout the whole brain ([Yang et al. \(2016\)](#)), the sulc and curvature in our conclusion displayed opposite trends in both shared and unique clusters. Possible explanations to this are many folds: Firstly, all of our gyral peaks are defined within the gyri, and the correlation between sulc and curvature within the gyri is much weaker than that in the whole brain. In addition, the correlation between sulc and curvature in some areas is very low, such as the anterior cingulate (most are shared peaks), dorsolateral frontal cortex (most are unique peaks), and middle temporal gyrus (most are unique peaks) ([Schmitt et al. \(2021\)](#)). This non-uniform spatial distribution leads to the disappearance of the correlation between sulc and curvature. Therefore, the anatomical patterns within the peaks and the global patterns of the entire brain are not in conflict.

Through evaluating the structural and functional connectivity properties of shared and unique peaks, we observed that shared peaks exhibit larger connectivity attributes, such as degree, strength, clustering coefficient, betweenness and efficiency, compared to unique peaks. Higher

degree and strength values suggest that shared peaks are connected to more vertices in the brain network. Additionally, we found that clustering coefficient and efficiency, which measure local information transmission capacity and resilience to random attacks in a network, were higher in shared peaks. Betweenness, a centrality measure that quantifies the importance of a node in the network, also showed higher values for shared peaks, indicating greater importance of these peaks in the brain network. These results suggest that shared peaks may play a role as network hubs in contrast to unique peaks. Gyrar peaks exhibit a high degree of connectivity within local neighborhoods, creating a “small world” structure within the network, and may behave as hubs in the structural/functional network, as suggested by previous studies ([Sporns and Zwi \(2004\)](#); [Bassett and Bullmore \(2006\)](#); [Bullmore and Sporns \(2009\)](#); [He and Evans \(2010\)](#)). In many studies, higher-order brain regions like the DMN are recognized as the global network hubs and the communication centers of the brain’s global network. These regions typically exhibit higher node degree and strength. However, there is an interesting finding in our study. In the human brain, the more shared peaks (about 65%) are located in lower-order brain regions, while unique peaks are mainly (about 74%) located in higher-order regions. However, this trend is relatively less pronounced in the macaque brain. There are two possible explanations for this. Firstly, peaks is defined at a much more local scale, in contrast to the definition of brain functional regions, such as DMN. This seemingly contradictory findings could be reconciled by their definitions of “network hubs” at respective coarse and fine scales. Specifically, while higher-order brain regions such as DMN serve as the information exchange centers for large-scale brain network, the information transfer within each region at a finer scale could be primarily facilitated by loci, such as the shared peak. These findings suggest that, peaks that are in larger-scale DMN while exhibiting lower hub-like attributes at a vertex-level, could be referred to as provincial hubs ([Guimera and Nunes Amaral \(2005\)](#); [Hwang et al. \(2017\)](#)). This can be understood as the preservation of the most fundamental and mainstream topological structure and communication patterns during the evolutionary process of species, while species-specific peaks that appear later in the evolutionary process may serve higher-order and more specific functions ([Goulas et al. \(2014\)](#); [Rilling \(2006\)](#)). Another issue worth discussing is the relationship between degree and clustering coefficient. Some studies focusing on social networks and random intersection graph models have found that clustering coefficient correlates negatively with degree ([Foudalis et al. \(2011\)](#); [Bloznelis \(2013\)](#)). While in our study, when comparing the functional network characteristics of shared and unique peaks, we found that the patterns of degree and clustering coefficient were similar (3). The differences in network characteristics between brain networks and social networks or random networks may reflect distinct organizational patterns in the brain compared to other networks. Furthermore, due to our focus on the internal properties of peaks in our study, the patterns observed may not align entirely with the principles followed by the entire brain network. Through comparisons with multiple brain atlases, we observed that there are more diverse brain regions around shared peaks than around unique peaks for multiple brain atlases with a median parcellation resolution. It is noted that the observation is not consistent on atlases with relatively lower resolutions (e.g., BA05 for macaque, $n=30$ and Yeo2011 for human, $n=7$) or, in particular, higher resolutions (e.g., Schaefer-500, and Vosdewael-400, $n>300$). This inconsistency is reasonable since the resolution of the parcellation itself will largely determines the chance of a cortical region appear in a peak’s neighborhood, if the parcellation resolution is too coarse or too fine. For example, if $n=1$ (the entire cortex is the only one region) or $n=30k$ (each vertex is a region), each peak will has the same number of neighboring regions for these two extreme cases (one brain region for each peak for $n=1$; around 30 vertices for each peak for $n=30k$). This finding may suggest a higher diversity of brain functions associated with shared peaks. From a microscopic perspective, brain function is determined by the structure and functional characteristics of cells. The brain is composed of various types of cells, and each type of cell contributes to different aspects of brain function. The differential expansion of cortical regions and the introduction of new functional modules during the process of evolution may be the result of changes in progenitor cells ([Clowry et al. \(2018\)](#)). In our experiment, the shared peaks represent regions with less cortical expansion, indicating a smaller proportion of ancestral cells. This may allow them to participate in a greater variety of brain functions and be surrounded by

more diverse brain regions. From a macroscopic perspective, in the analysis of brain folding, a traditional approach is to partition the brain into a set of distinct regions, known as parcellation, based on functional, structural, or cytoarchitectural criteria. This parcellation serves as the most common unit of analysis in studying brain folds. This well-defined partitioning method provides an intuitive framework for analyzing the brain, leading to computational, statistical, and interpretational efficiencies [Eickhoff et al. \(2018\)](#); [Glasser et al. \(2016\)](#). Simply averaging all vertex characteristics within a region assumes the homogeneity within the region and only one dominant pattern [Haak and Beckmann \(2020\)](#). However, both functional and microstructural properties often highly variable within a region, and inconsistent across modalities. Additionally, adjacent vertices in different regions may also have similar characteristics. Therefore, boundaries vary depending on the chosen modality, and no clear boundaries are evident in all modalities or analysis approaches. The brain has no true ‘boundaries’. In our study, we observed that shared peaks in regions surrounded by a larger number of neighboring brain regions are more likely to be assigned to the ‘boundaries’ of those regions across different classification approaches. Therefore, we speculate that these shared peaks might be involved in a more diverse range of brain functions.

Using lasso regression, we screened the genes on the cortex and identified 28 genes that made significant contributions to the classification of shared and unique peaks. Further applying Welch’s t-test, we found significant differential expression in 7 genes between the shared and unique peak regions. Among them, SNAP29 and KCNH5 are closely associated with neuronal activity and brain function, and these two genes show higher and lower expression levels in the shared peaks, respectively. While, low expression of SNAP29 protein levels disrupts neural circuits in a presynaptic manner, leading to behavioral dysfunctions [Yan et al. \(2021\)](#). Therefore, the majority of shared peaks located in lower-level brain regions exhibit higher SNAP29 expression, aiming to minimize the occurrence of low SNAP29 expression that could disrupt neural circuits and result in behavioral dysfunctions. Another differentially expressed gene was KCNH5. The voltage-gated Kv10.2 potassium channel, encoded by KCNH5, is broadly expressed in mammalian tissues, including the brain. According to previous studies, dysfunction of Kv10.2 may be associated with epileptic encephalopathies and autism spectrum disorder (ASD) [\(Hu et al. \(2022\)\)](#). And these two diseases happen to be more prevalent in humans, coinciding with the high expression of the KCNH5 gene in unique peaks.

Materials and Methods

Dataset Description

Human MRI

In our study, we utilized the Human Connectome Project (HCP) S900 Subjects MR imaging data from Q3 Release (<https://www.humanconnectome.org/>). The data was obtained from the Q3 Release and all participants involved provided written informed consent and the study was approved by the relevant institutional review boards. The MR images were acquired by a Siemens ‘Connectome Skyra’ 3T scanner housed at Washington University in St Louis using a 32-channel head coil. For T1-weighted MRI: TR=2400 ms, TE=2.14 ms, flip angle=8 deg, FOV=224× 224 mm and resolution= 0.7×0.7×0.7 mm³. T2-weighted MRI: TR=3200 ms, TE=565 ms and resolution=0.7×0.7×0.7 mm³. Diffusion MRI (dMRI): TR=5520 ms, TE=89.5 ms, refocusing flip angle=160 deg, flip angle=78 deg, FOV=210×180 mm, matrix=168×144, resolution=1.25×1.25×1.25 mm³, 1.25 mm isotropic voxels, echo spacing=0.78 ms, BW=1488 Hz/Px. Resting state fMRI (rfMRI): TR=720 ms, TE=33.1 ms, flip angle=52 deg, FOV=208×180 mm, matrix=104×90, 1200 time points, 2.0 mm isotropic voxels, BW=2290 Hz/Px.

We applied the standard HCP MR structural pipelines ([Glasser et al. \(2013\)](#); [Fischl \(2012\)](#); [Jenkinson et al. \(2002\)](#), 2012)) for processing all structural MR images. This involved the following three main steps: 1) PreFreeSurfer pipeline ([Jovicich et al. \(2006\)](#); [Van der Kouwe et al. \(2008\)](#); [Smith \(2002\)](#)) which corrected for image distortion, aligned and averaged T1w and T2w images and registered the subject's native structural volume space to MNI space. 2) FreeSurfer pipeline ([Dale et al. \(1999\)](#); [Fischl et al. \(1999\)](#), 2002); [Ségonne et al. \(2005\)](#)) including segmentation of brain volume, reconstruction of white matter and pial surfaces, and registering to fsaverage surface atlas; 3) PostFreeSurfer pipeline, including surface registration to the Conte69 surface template ([Van Essen et al. \(2012b\)](#)) by using MSM-All algorithm ([Glasser et al. \(2016\)](#); [Robinson et al. \(2014\)](#), 2018)). In this step, cortical folding, myelin maps, and resting state fMRI (rfMRI) correlations together for registration, which improved the cortical correspondences across different subjects. For our study, the white matter cortical surface with 64,984 vertices after MSM-All registration and the associated cortical folding features such as sulc, myelin, and cortical thickness, were adopted for cross-subjects analysis. For the diffusion MRI (dMRI) data, we performed fiber tractography using MRtrix3 ([Tournier et al. \(2019\)](#), <https://www.mrtrix.org>). Each individual had 40,000 fiber tracts reconstructed. A maximum length limit of 150mm was defined to reduce the presence of false positives ([Varriano et al. \(2018\)](#)).

Gene Expression Data

The AHBA microarray gene expression data consists of 3702 samples from 6 typical adult human brains. Several hundred samples (mean \pm standard deviation: 617 \pm 241) were collected from cortical, subcortical, brainstem and cerebellar regions in each brain to profile genome-wide gene expression. In the AHBA, each gene probe is associated with a numerical ID and a platform-specific label or name. If a probe is assigned to represent a unique gene it is also characterized with a range of gene-specific labels such as gene symbol and an Entrez Gene ID—a stable identifier for a gene generated by the Entrez Gene database at the National Center for Biotechnology Information (NCBI). The probe-level data offer high-resolution coverage of nearly the entire brain, providing expression measures for over 20,000 genes from 3702 spatially distinct tissue samples. The AHBA data is available at figshare <https://figshare.com/s/441295fe494375aa0c13>. The AHBA dataset has been preprocessed, and detailed information can be referred to ([Arnatkevičiūtė et al. \(2019\)](#)). The first six processing steps produce the region \times gene matrix that can be used for the regional analyses.

Macaques MRI

We selected rhesus macaque monkeys' structural and functional MR imaging data aging from 0.8–4.5 years from the non-human primate (NHP) consortium PRIME-DE from University of Wisconsin–Madison (http://fcon_1000.projects.nitrc.org/indi/prime.html). The full dataset consisted of 592 rhesus macaque monkeys (*Macaca mulatta*) scanned on a 3T with a 4-channel coil. For T1-weighted MRI: TR=11.4 ms, TE=5.41 ms, flip angle=10 deg, image matrix=512 \times 248 \times 512 and resolution=0.27 \times 0.50 \times 0.27 mm³. The rsfMRI data were preprocessed based on DPARSF, which included slice timing, realignment, covariant regression, band-pass filtering (0.01–0.1 Hz), and smoothing (FWHM=4 mm). We fed T1w images to CIVET, registering it into the NMT-standardized space ([Seidlitz et al. \(2018\)](#)) using an affine transformation, followed by image resampling and tissue segmentation. The reconstructed white matter cortical surface was obtained using FreeSurfer. We resampled the surfaces to 40k vertices to ensure vertex-to-vertex correspondence across subjects by spherical registration. After linear registration between fMRI and T1w MRI via FLIRT, we mapped the volume time-series to surface vertices for further analysis.

Peak Cluster Extraction

Based on our previous work, gyral peaks are defined as the highest point of the gyri ([Zhang et al. \(2022\)](#)). Gyral height was measured by “Sulc” (<https://surfer.nmr.mgh.harvard.edu/>, [Fischl \(2012\)](#)), which was defined as the displacement from a vertex on the surface to a hypothetical

mid-surface, which is between the gyri and sulci, and the ‘mean’ of displacements of all vertices is zero ([Fischl et al. \(1999\)](#)). Thus, gyral peaks on individuals were identified by locating the vertex of the minimum sulc value within the x-ring (4-ring for humans, 3-ring for macaques) neighborhood on the grid ([Zhang et al. \(2022\)](#), [2023](#)). To obtain group-wise peak clusters, all gyral peaks in individual spaces of the two species were projected onto the respective template white matter surface, which produced a count map of peaks for each species. Of note, vertex-to-vertex correspondences were established across all surfaces within each species. Next, peak count maps of two species were processed by anisotropic smoothing, with n iterations within an k -ring neighborhood, as described in ([Meng et al. \(2014\)](#); [Zhang et al. \(2023\)](#)). Finally, we applied the watershed clustering algorithm, as detailed in ([Meng et al. \(2014\)](#); [Rettmann et al. \(2002\)](#); [Yang and Kruggel \(2008\)](#); [Zhang et al. \(2023\)](#)) to the smoothed count map to automatically generate group-wise peak clusters for each species. Notably, the selection of parameters for anisotropic smoothing and watershed clustering algorithm were based on the previous work ([Zhang et al. \(2022\)](#), [2023](#)). Parameters of these three steps (individual peak extraction, anisotropic smoothing and watershed clustering algorithm) on two species are reported in the Supplementary Information. In total, 192 (LH: 96, RH: 96) and 85 (LH: 42, RH: 43) peak clusters were detected on Humans and macaques, respectively (**Figure. 1** (a)).

Cross-species Registration

To elucidate the inter-species relationship of group gyral peaks between humans and macaques, a functional joint alignment technique ([Xu et al. \(2020\)](#)) was employed to project macaque peak clusters onto the human cortical surface. They first constructed a joint similarity matrix by concatenating within- and cross-species similarities of connectivity patterns. Next, the diffusion embedding algorithm applied on the similarity matrix. Finally, we use gradients as surface features and align the cortical surfaces of humans and macaques using Multimodal Surface Matching (MSM) ([Robinson et al. \(2014\)](#)). This technique builds upon recent advances in high-dimensional common space representations of functional organization and offers a transformational framework between human and macaque cortices.

Definition of Shared and Unique Peak Clusters

After the cross-species registration mentioned above, the group-wise gyral peak clusters of the two species were placed on the same template surface. The determination of peak clusters that are shared between species involves two criteria: 1) the Dice of clusters > 0 ; and 2) the geodesic distance between the centers of the two clusters is less than 7 mm. If a pair of clusters satisfies either one of these two criteria, they can be identified as peak clusters that are shared between species. The difference set between all peaks of the two species and the shared peaks is the set of unique peaks for each species.

Statistic Analysis

All variables used in the two-samples t-test follow a normal distribution and all p-values were corrected for multiple comparisons using the false discovery rate (FDR) method. Moreover, in order to identify differently expressed genes within shared and unique peaks, and considering the unequal sample sizes for shared and unique peaks, we employed the Welch’s t-test, which is suitable for this scenario. For all tests, a p-value < 0.05 was considered significant (FDR corrected).

Anatomical Features of Gyral Peaks

We analyzed the anatomical characteristics of shared and unique gyral peaks, including sulc, curvature (the amount of bending at a point on a convoluted surface), thickness (the distance from the point on the pial surface to the nearest point on the white surface ([Fischl and Dale \(2000\)](#))).

myelin, and local surface area (We calculate that the average area of all triangles in the neighborhood of vertex i is S_i . The local surface area of vertex i is the mean neighborhood area S_i divided by the mean of all vertices in the whole brain).

Functional and Structural connectivity

We parcellated the white matter surface (excluded the regions between two hemispheres) into 1400 patches for human and 1700 patches for macaque ([He et al. \(2022\)](#)) due to the number of vertices on the surface. We constructed a structural connective graph $G_s = \{V, E_s, A_s\}$ and a functional connective graph $G_f = \{V, E_f, A_f\}$ for each subject. Graph nodes v_s and v_f were defined as cortical patches of the same area. For human individual structural connectivity matrix A , a_s^{ij} represents the fiber count connecting the two nodes. For human and macaque individual functional connectivity matrix, we calculate the Pearson correlation coefficient (PCC) between the average time-series between two nodes v^t and v^f , followed by Fisher's z-transformation. Due to the vertex-to-vertex correspondences across individual surfaces of each species, the patches (or nodes) had cross-subject correspondences as well. On this basis, we averaged the structural and functional connectivity matrix of each subject to obtain a group-average structural and functional connectivity matrix \bar{A}_s and \bar{A}_f . Then, for each row in the group-average functional connectivity matrix, the values of the top 10% of connections were retained, whereas all others were zeroed. On this group-average graph, we computed nodal graph metrics, including degree, strength, clustering coefficient, betweenness, and efficiency via Brain Connectome Toolkit (<https://sites.google.com/site/bctnet/>). The definitions of these network properties are detailed in the Supplementary Information.

Feature selection of genes

Since we divided human gyral peaks into peaks shared with macaque and peaks unique to human, we aimed to investigate the genes that are significantly different expressed between two types of gyral peak. The preprocessed AHBA gene data is in the form of region×gene and the region above referred to the parcellation of a certain atlas, such as Aparc, Schaefer100, Schaefer500, Schaefer1000, etc. We finally selected Schaefer500 atlas for this study because high resolution may result in some areas with no gene data (more details refer to [Arnatkevičiūtė et al. \(2019\)](#)), while low resolution may result in multiple categories of clusters being located in the same region. Therefore, Schaefer500 was chosen as the most suitable atlas for our analysis. We first labeled all regions of Schaefer500 as shared, unique, or other based on the positions of group-wise gyral peaks. Then, Lasso (a linear regression method that uses L1 regularization for gene selection) was applied on this labeled gene data. The cost function of Lasso regression is as follows:

$$Cost(w) = \sum_{i=1}^N (y_i - w^T x_i)^2 + \lambda ||w||$$
An important parameter of Lasso is lambda, which affects the sparsity of feature selection. We used 10-fold cross-validation to select the optimal lambda. By considering the maximization of accuracy (acc) and minimization of mean squared error (MSE) simultaneously, the lambda value was ultimately determined to be 0.027 (**Figure. 5** (b)). The accuracy of training set was 0.84, and the MSE was 0.64; The accuracy of test set was 0.75, and the MSE was 1.00.

Data availability

All human data analyzed in this manuscript were obtained from the open-access HCP adult sample (<https://www.humanconnectome.org/>). Macaque data came from PRIME-DE (http://fcon_1000.projects.nitrc.org/indi/indiPRIME.html). Fiber tracking based on MRtrix3 (<https://www.mrtrix.org>).

Acknowledgements

We would like to thank the various contributors to the open access databases that our data was downloaded from. HCP data were provided by the Human Connectome Project, WU-Minn Consortium (Principal Investigators: David Van Essen and Kamil Ugurbil; 1U54MH091657) funded by the 16 NIH Institutes and Centers that support the NIH Blueprint for Neuroscience Research; and by the McDonnell Center for Systems Neuroscience at Washington University. Macaque data were provided by the PRIME-DE. Primary support for the work by Michael P. Milham and the INDI team was provided by gifts from Joseph P. Healy to the Child Mind Institute, as well as by the BRAIN Initiative (R01MH111439). MPM is a Randolph Cowen and Phyllis Green Scholar. Primary support for the work by Charles Schroeder is provided by the BRAIN Initiative (R01MH111439) and the Sylvio O. Conte Center ‘Neurobiology and Dynamics of Active Sensing’ (P50MH109429). Primary support for the work by Daniel Margulies is provided by the Max Planck Society.

Additional information

Funding

Funder	Grant reference number	Author
National Natural Science Foundation of China	31971288	Tuo Zhang
Key Program of the National Natural Science Foundation of China	62131009	Tuo Zhang
Innovation Foundation for Doctor Dissertation of Northwestern Polytechnical University	CX2022053	Songyao Zhang
Innovation Foundation for Doctor Dissertation of Northwestern Polytechnical University	CX2022052	Zhibin He
National Key R&D Program of China	2020AAA0105701	Junwei Han
National Natural Science Foundation of China	61936007	Junwei Han
National Natural Science Foundation of China	U20B2065	Junwei Han
National Natural Science Foundation of China	U1801265	Junwei Han
National Natural Science Foundation of China	61936007	Lei Guo
The funders had no role in study design, data collection and interpretation, or the decision to submit the work for publication.		

Appendix

Parameter selection

Table A1 [↗](#) presents all the parameters used in the three algorithms for detecting individual and group peaks in the two species, along with their corresponding meanings. We used x-order ring neighbor to detect peaks on individual surfaces and chose k-order ring plus n-iterations for anisotropic smooth algorithm for the count map. Parameters for watershed clustering algorithm are related to the value of the count map. fg and bg respectively determine the minimum and maximum count of the segmented area. A smaller value of parameter merge results in more clusters. All parameters were determined based on previous studies (*Zhang et al. (2022, 2023)*).

Assignments	Parameters	Meanings	Human	Macaque
Detect Individual Peaks	x	Search peaks ring	4	3
Anisotropic Smooth	k	Anisotropic Smooth ring	1	1
	n	Smooth iteration	20	20
Watershed Clustering	fg	Minimum count value for cluster coverage	45	4
	bg	Maximum count value for cluster coverage	209	28
	merge	Determinants of whether two clusters are merged	7	3

Table A1.
Parameter selection of gyral peaks detection in human and macaque.

Locations of Peaks in Human and Macaque

Table A2 [↗](#) and **Table A3** [↗](#) displays the locations of all peaks in the human and macaque brain. The region names are derived from the *aparc2009* atlas of human and *BA05* atlas of macaque.

Locations of Shared and Unique Peak Clusters

Figure A1 [↗](#) shows the locations of shared peak clusters of macaque on the surface of the macaque brain template. The locations of all human shared peaks are reported in **Table A4** [↗](#).

The main text presents the counts of peak cluster centers occurrence in different networks (Cole-Anticevic). In order to eliminate the influence of different brain area sizes on the count of cluster, we normalized the count by the regional surface area and reported in **Figure. A2** [↗](#). The results were similar to those on the original counts. Our findings indicated that most of the shared peaks are located in low-order sensory and motor networks, while most of the unique peaks are located in higher-order networks. The regions with the highest density of shared peak cluster centers are V1, Aud, and VMN, while the region with the highest density of unique peak cluster centers is Lan, DMN, OAN, and FPN. Further explanations of some of the different observations in **Figure. 2** [↗](#) and **Figure. A2** [↗](#) can be found in the ‘Discussion and Conclusion’ section.

Confidence of Shared Peaks

Figure. A3 [↗](#) (a) illustrates the locations of all shared peaks. There are two definitions of shared peaks:

1) the Dice of clusters > 0; and 2) the geodesic distance between the centers of the two clusters is less than 7mm. The credibility of shared peak clusters defined by the coincidence rate of clusters is measured using the overlap ratio. The higher the overlap rate of clusters, the higher the confidence of shared clusters between species **Figure. A3** [↗](#) (b). The credibility of shared peak clusters defined by the distance of cluster centers is measured using the ranking of center distances. The distance between the two closest clusters in the whole brain is set as 100 points, and the distances of other clusters are proportionally reduced accordingly **Figure. A3** [↗](#) (c).

Network properties for graph analysis

Network Properties

Degree

Degree is the most important description of the statistical characteristics of node connection. Degree K_i is defined as the number of edges directly connected to a node i . The greater the degree of the node, the more connections the node has, and the more important the status of the node in the network. G is an undirected weighted network in our work, the degree of node i is defined as:

$$K_i = \sum_{j=1}^N a_{ij} \quad (1)$$

Strength

For a N -node weighted network G which weight matrix is W , the strength of node i is defined as:

$$S_i = \sum_{j=1}^N w_{ij} \quad (2)$$

Location	Human Cluster Number	Location	Human Cluster Number
G_and_S_frontomargin	61	G_oc-temp_med-Parahip	3,9,15,63,74,108
G_and_S_occipital_inf	120,130	G_orbital	20,25,52,55,60,62,64,69,92,113
G_and_S_paracentral	2,28	G_pariet_inf-Angular	175,189
G_and_S_subcentral	23,38	G_pariet_inf-Supramar	156,171,172
G_and_S_transv_frontopol	51,182	G_parietal_sup	140,178,185,187
G_and_S_cingul-Ant	40,44,89,105,115,162,186	G_postcentral	33,35,99,109,124,139,153,170
G_and_S_cingul-Mid-Ant	49,70,72,158	G_precentral	18,39,53,65,66,67,87,90,107
G_and_S_cingul-Mid-Post	45,79	G_precuneus	88,100,117,143,180,192
G_cingul-Post-dorsal	26,37,78,98,102	G_rectus	7,13,22,27,41,82
G_cingul-Post-ventral	29,150,154	G_temp_sup-Lateral	47,59,68,81,93,114,116
G_cuneus	21,31,34,36	G_temporal_inf	95,123,128,160
G_front_inf-Opercular	42,43,125	G_temporal_middle	76,104,112,129,173
G_front_inf-Orbital	80	Pole_occipital	1,11,17,24,57,142
G_front_inf-Triangul	132,135,138	Pole_temporal	6,14,106,141,146
G_front_middle	131,149,152,165,179,184,188	S_calcarine	83
G_front_sup	46,71,73,75,77,84,85,91,97,118, 126,137,157,161,174,181,183,191	S_front_middle	190
G_Ins_Ig_and_S_cent_ins	16,32,54,119	S_front_sup	166,169
G_insular_short	4,12	S_intrapariet_and_P_trans	159
G_occipital_middle	101,110,121,127,155	S_oc-temp_med_and_Lingual	151
G_occipital_sup	96,103,144,145	S_orbital-H_Shaped	122
G_oc-temp_lat-fusifor	48,58,147,163,164,167	S_pericallosal	50,94
G_oc-temp_med-Lingual	8,10,19,56,133,134,136,148,168, 176,177	S_subparietal	111

Table A2.

The location of human peak clusters.

Location	Macaque Cluster Number	Location	Macaque Cluster Number
Area 2	11,15,37,43,48	Area 13	5,7,10,13,16,46,49,54,77
Area 3	4,32,33,69,74	Area 14	31,34,50,55,83
Area 4	9,27,56,70,71	Area 15	25,26
Area 5	1,44	Area 16	14,42,79,85
Area 6	22,35,58,80	Area 20	3,18,38,39,41,47,51,57,61,62,63
Area 7	2,6,12,17,28,45,53,60,65,67,76,82	Area 21	8,23,24,30,40,64,66,81
Area 9	19,29,68,72	Area 23	75
Area 12	20,21,52,59,73,84	Area 24	36,78

Table A3.

The location of macaque peak clusters.

Shared Peak Clusters of Macaque

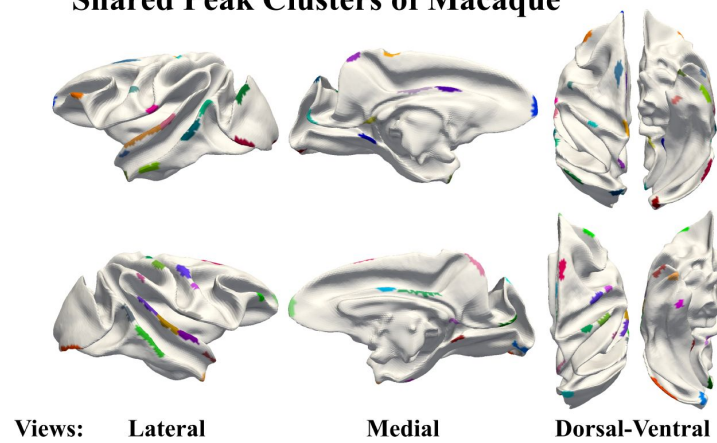


Figure A1.

Macaques share peak clusters display on the surface of the macaque brain template.

Clusters in LH	Location	Clusters in RH	Location
LH Shared 1	G_front_sup	RH Shared 1	G_and_S_transv_frontopol
LH Shared 2	G_and_S_subcentral	RH Shared 2	G_postcentral
LH Shared 3	G_cuneus	RH Shared 3	G_temp_sup-Lateral
LH Shared 4	G_oc-temp_med-Parahip	RH Shared 4	G_occipital_sup
LH Shared 5	G_temp_sup-Lateral	RH Shared 5	G_orbital
LH Shared 6	G_occipital_middle	RH Shared 6	Pole_temporal
LH Shared 7	G_precentral	RH Shared 7	Pole_occipital
LH Shared 8	G_temp_sup-Lateral	RH Shared 8	G_front_inf-Opercular
LH Shared 9	G_orbital	RH Shared 9	G_temp_sup-Lateral
LH Shared 10	G_postcentral	RH Shared 10	G_oc-temp_med-Parahip
LH Shared 11	Pole_temporal	RH Shared 11	G_precentral
LH Shared 12	G_and_S_cingul-Mid-Ant	RH Shared 12	Pole_occipital
LH Shared 13	G_oc-temp_med-Lingual	RH Shared 13	G_occipital_middle
LH Shared 14	G_parietal_sup	RH Shared 14	G_postcentral
LH Shared 15	G_oc-temp_med-Lingual	RH Shared 15	Pole_occipital
LH Shared 16	Pole_occipital	RH Shared 16	G_precuneus
LH Shared 17	G_oc-temp_med-Parahip	RH Shared 17	G_precentral
LH Shared 18	G_and_S_occipital_inf	RH Shared 18	G_pariet_inf-Supramar
LH Shared 19	S_front_sup	RH Shared 19	G_front_sup
LH Shared 20	Pole_temporal	RH Shared 20	Unkown
LH Shared 21	G_precentral	RH Shared 21	G_temp_sup-Lateral
LH Shared 22	G_cingul-Post-ventral	RH Shared 22	G_cingul-Post-ventral
LH Shared 23	Pole_occipital	RH Shared 23	G_and_S_cingul-Mid-Ant
LH Shared 24	Pole_occipital	RH Shared 24	G_oc-temp_lat-fusifor
LH Shared 25	G_and_S_cingul-Mid-Ant	RH Shared 25	G_oc-temp_med-Lingual
		RH Shared 26	G_and_S_cingul-Mid-Post

Table A4.

Location of shared peak clusters on human.

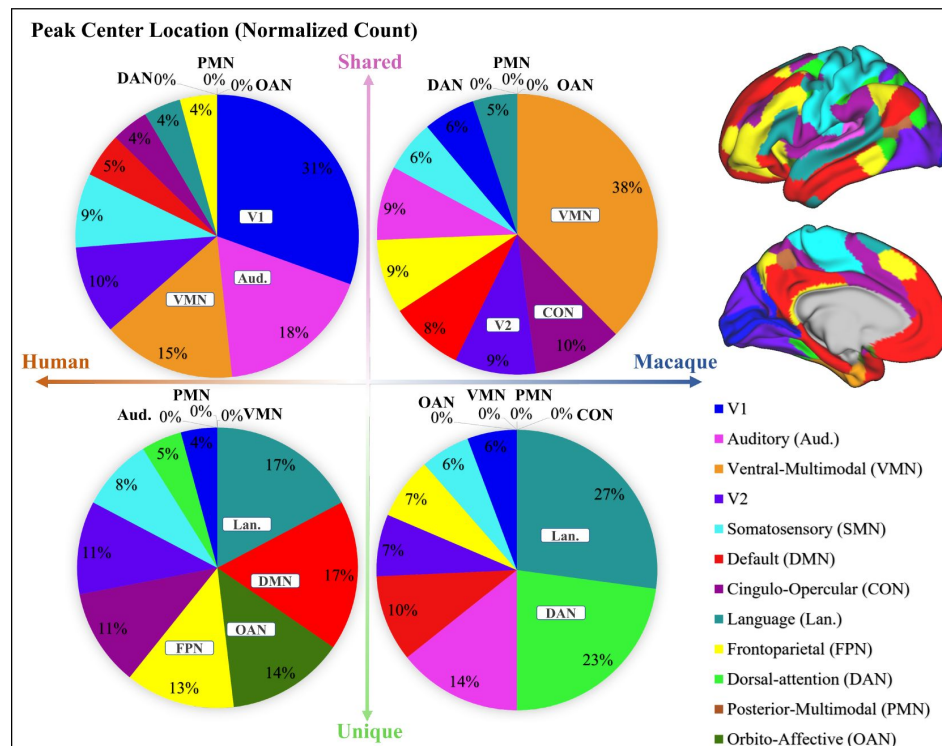


Figure A2.

Pie chart shows the normalized count of shared and unique peaks across different brain networks both for human and macaque. Right panel shows the Cole-Anticevic (CA) networks (*Ji et al. (2019)*) on human surface as a reference.

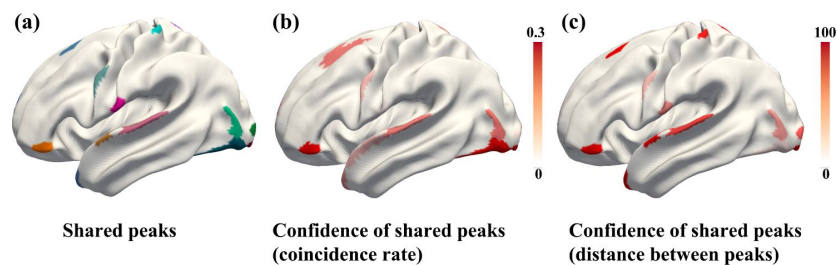


Figure A3.

(a) Location of shared peaks. (b) Confidence of shared peak clusters defined by the coincidence rate of clusters between human and macaque. (c) Confidence of shared peak clusters defined by the distance of cluster centers between human and macaque.

Cluster Coefficient

The clustering coefficient of a vertex i is the probability that the neighbours of this vertex (all other vertices to which it is connected by an edge) are also connected to each other. The clustering coefficient of a vertex ranges between 0 and 1.

$$C_i = \frac{2e_i}{k_i(k_i - 1)} = \frac{\sum_{j,m} a_{ij}a_{im}a_{mj}}{k_i(k_i - 1)} \quad (3)$$

Betweenness Centrality

Betweenness Centrality indicates the times of a node appears on all shortest paths in a graph. σ_{st} is the number of shortest paths from node s to node t , and $\sigma_{st}(v_i)$ is the number of times those paths pass through (v_i) .

$$BC_i = \sum_{s \neq i \neq t} \frac{\sigma_{st}(v_i)}{\sigma_{st}} \quad (4)$$

Efficiency

The average communication efficiency of the network G is then defined as the average over the pairwise efficiencies:

$$E(i) = \frac{1}{N_{G_i}(N_{G_i} - 1)} \sum_{j \neq k \in G_i} \frac{1}{l_{j,k}}, \quad (5)$$

Structural connectivity

Spatial Relationship Between Peaks and Functional Regions

We conducted a statistical analysis of the number of functional brain regions appearing in the neighborhoods of shared and unique peaks. The outcomes, derived from the utilization of comprehensive human brain atlases, were summarized in **Table A6** [↗](#).

List of Genes Selected by Lasso

	Degree	Strength	CC	Betweenness	Efficiency
Shared	31.37±5.04	32.29±5.79	0.23±0.04	5.50±2.12(×10³)	0.43±0.05
Unique	31.79±3.23	29.46±3.43	0.19±0.02	5.10±1.08(×10 ³)	0.39±0.03
p	<0.01	<0.001	<0.001	<0.001	<0.001
t	2.39	9.08	23.01	5.66	21.20

Table A5.

The mean (±SD) structural connectivity characteristics of shared and unique peak clusters of human. The bold font represent the larger values between the shared peak and unique peaks. *indicates p<0.05; **indicates p<0.01, ***indicates p<0.001

Atlas Name	Yeo2011(7)	Glasser2016	Schaefer-100	Schaefer-200	Schaefer-300	Schaefer-400	Schaefer-500
Share Nbr	1.48±0.10	2.43±0.15	1.89±0.12	2.12±0.11	2.23±0.11	2.46±0.13	2.50±0.14
Unique Nbr	1.54±0.07	2.37±0.09	1.74±0.09	2.08±0.10	2.17±0.10	2.39±0.09	2.51±0.09
p	<0.001	<0.001	<0.001	<0.001	<0.001	<0.001	<0.001
t	-8.04	8.32	26.66	4.50	18.08	17.60	7.72
Atlas Name	Schaefer-600	Schaefer-700	Schaefer-800	Schaefer-900	Schaefer-1000	Vosdewael-100	Vosdewael-200
Share Nbr	2.48±0.14	2.76±0.14	2.85±0.16	2.86±0.12	3.07±0.14	1.57±0.17	1.71±0.11
Unique Nbr	2.60±0.10	2.74±0.10	2.74±0.12	2.87±0.09	3.03±0.10	1.46±0.10	1.73±0.08
p	<0.001	0.39	<0.001	<0.001	<0.001	<0.001	<0.001
t	-14.04	2.42	11.98	-5.75	4.23	34.09	7.44
Atlas Name	Vosdewael-300	Vosdewael-400	Yeo2011(17)	Aparc	Aparc2009	BA	Cole-Anticevic
Share Nbr	1.96±0.12	2.21±0.15	1.76±0.11	1.58±0.12	1.95±0.13	1.58±0.12	1.65±0.11
Unique Nbr	2.02±0.09	2.32±0.10	1.73±0.08	1.33±0.07	1.94±0.09	1.29±0.08	1.57±0.07
p	<0.001	0.13	<0.001	<0.001	<0.001	<0.001	<0.001
t	5.41	-2.82	22.29	56.37	3.80	69.84	22.44

Table A6.

The mean values (±SD) of brain regions where shared and unique peaks appeared within a 3-ring neighborhood in 21 common human atlases. The p-values were corrected by FDR.

Gene Symbol	p	Gene Symbol	p	Gene Symbol	p	Gene Symbol	p
INPP4A	0.76	TLR1	0.02	KCNH5	0.04	OTULIN	0.18
ITGA1	0.19	TPST1	0.94	TMEM248	0.27	DTX2	0.15
JUNB	0.57	SNAP29	0.01	ANO2	0.26	SERPINB9P1	0.12
PECAM1	0.04	TRAM2	0.70	PLEKHA3	0.90	LHFPL5	0.63
PRKCH	0.10	DHRS4	0.05	PLBD1	0.01	GK5	0.51
NECTIN1	0.84	LPIN1	0.34	DENND1C	0.37	ZNF662	0.77
SRC	0.20	BHMT2	0.01	CXXC4	0.20	NAP1L6	0.58

Table A7.

The 28 genes selected by LASSO and their corresponding p-values from Welch's t-test.

References

1. Arnatkevičiūtė A, Fulcher BD, Fornito A (2019) **A practical guide to linking brain-wide gene expression and neuroimaging data** *Neuroimage* **189**:353–367
2. Barks SK, Parr LA, Rilling JK (2015) **The default mode network in chimpanzees (Pan troglodytes) is similar to that of humans** *Cerebral cortex* **25**:538–544
3. Bassett DS, Bullmore E (2006) **Small-world brain networks** *The neuroscientist* **12**:512–523
4. Bloznelis M. (2013) **Degree and clustering coefficient in sparse random intersection graphs**
5. Buckner RL, Andrews-Hanna JR, Schacter DL (2008) **The brain's default network: anatomy, function, and relevance to disease** *Annals of the new York Academy of Sciences* **1124**:1–38
6. Buckner RL, Krienen FM (2013) **The evolution of distributed association networks in the human brain** *Trends in cognitive sciences* **17**:648–665
7. Buckner RL, Krienen FM, Yeo BT (2013) **Opportunities and limitations of intrinsic functional connectivity MRI** *Nature neuroscience* **16**:832–837
8. Bullmore E, Sporns O (2009) **Complex brain networks: graph theoretical analysis of structural and functional systems** *Nature reviews neuroscience* **10**:186–198
9. Cachia A, Roell M, Mangin JF, Sun ZY, Jobert A, Braga L, Houde O, Dehaene S, Borst G (2018) **How interindividual differences in brain anatomy shape reading accuracy** *Brain Structure and Function* **223**:701–712
10. Caminiti R, Chafee MV, Battaglia-Mayer A, Averbach BB, Crowe DA, Georgopoulos AP (2010) **Understanding the parietal lobe syndrome from a neurophysiological and evolutionary perspective** *European Journal of Neuroscience* **31**:2320–2340
11. Clowry GJ, Alzu'bi A, Harkin LF, Sarma S, Kerwin J, Lindsay SJ (2018) **Charting the protomap of the human telencephalon** *Seminars in Cell & Developmental Biology* :3–14
12. Dale AM, Fischl B, Sereno MI (1999) **Cortical surface-based analysis: I. Segmentation and surface reconstruction** *Neuroimage* **9**:179–194
13. Eichert N, Verhagen L, Folloni D, Jbabdi S, Khrapitchev AA, Sibson NR, Mantini D, Sallet J, Mars RB (2019) **What is special about the human arcuate fasciculus? Lateralization, projections, and expansion** *cortex* **118**:107–115
14. Eickhoff SB, Yeo BT, Genon S (2018) **Imaging-based parcellations of the human brain** *Nature Reviews Neuroscience* **19**:672–686
15. Essen DCv (1997) **A tension-based theory of morphogenesis and compact wiring in the central nervous system** *Nature* **385**:313–318
16. Ferrier D (1873) **Experimental researches in cerebral physiology and pathology** *British Medical Journal* **1**

17. Fischl B (2012) **FreeSurfer** *Neuroimage* **62**:774–781
18. Fischl B, Dale AM (2000) **Measuring the thickness of the human cerebral cortex from magnetic resonance images** *Proceedings of the National Academy of Sciences* **97**:11050–11055
19. Fischl B *et al.* (2002) **Whole brain segmentation: automated labeling of neuroanatomical structures in the human brain** *Neuron* **33**:341–355
20. Fischl B, Sereno MI, Dale AM. (1999) **Cortical surface-based analysis: II: inflation, flattening, and a surface-based coordinate system** *Neuroimage* **9**:195–207
21. Fornito A, Yücel M, Wood S, Stuart GW, Buchanan JA, Proffitt T, Anderson V, Velakoulis D, Pantelis C (2004) **Individual differences in anterior cingulate/paracingulate morphology are related to executive functions in healthy males** *Cerebral cortex* **14**:424–431
22. Foudalis I, Jain K, Papadimitriou C, Sideri M. (2011) **Modeling social networks through user background and behavior** *Algorithms and Models for the Web Graph: 8th International Workshop, WAW 2011, Atlanta, GA, USA, May 27-29, 2011. Proceedings 8 Springer* :85–102
23. Friedrich P *et al.* (2021) **Imaging evolution of the primate brain: the next frontier?** *NeuroImage* **228**
24. Glasser MF *et al.* (2016) **A multi-modal parcellation of human cerebral cortex** *Nature*
25. Glasser MF *et al.* (2013) **The minimal preprocessing pipelines for the Human Connectome Project** *Neuroimage* **80**:105–124
26. Golesorkhi M, Gomez-Pilar J, Çatal Y, Tumati S, Yagoub MC, Stamatakis EA, Northoff G (2022) **From temporal to spatial topography: hierarchy of neural dynamics in higher-and lower-order networks shapes their complexity** *Cerebral Cortex* **32**:5637–5653
27. Gordon EM *et al.* (2023) **A somato-cognitive action network alternates with effector regions in motor cortex** *Nature* :1–9
28. Goulas A, Bastiani M, Bezgin G, Uylings HB, Roebroek A, Stiers P (2014) **Comparative analysis of the macroscale structural connectivity in the macaque and human brain** *PLoS computational biology* **10**
29. Guimera R (2005) **Nunes Amaral LA. Functional cartography of complex metabolic networks** *nature*
30. Haak KV, Beckmann CF (2020) **Understanding brain organisation in the face of functional heterogeneity and functional multiplicity** *NeuroImage* **220**
31. Hawrylycz MJ *et al.* (2012) **An anatomically comprehensive atlas of the adult human brain transcriptome** *Nature* **489**:391–399
32. He Y, Evans A (2010) **Graph theoretical modeling of brain connectivity** *Current opinion in neurology* **23**:341–350
33. He Z, Du L, Huang Y, Jiang X, Lv J, Guo L, Zhang S, Zhang T (2022) **Gyral hinges account for the highest cost and the highest communication capacity in a corticocortical network** *Cerebral Cortex* **32**:3359–3376

34. Hill J, Inder T, Neil J, Dierker D, Harwell J, Van Essen D (2010) **Similar patterns of cortical expansion during human development and evolution** *Proceedings of the National Academy of Sciences* **107**:13135–13140
35. Hopkins WD *et al.* (2014) **Evolution of the central sulcus morphology in primates** *Brain, behavior and evolution* **84**:19–30
36. Hu X, Yang J, Zhang M, Fang T, Gao Q, Liu X. (2022) **Clinical Feature, Treatment, and KCNH5 Mutations in Epilepsy** *Frontiers in Pediatrics* **10**
37. Hwang K, Bertolero MA, Liu WB, D’Esposito M (2017) **The human thalamus is an integrative hub for functional brain networks** *Journal of Neuroscience* **37**:5594–5607
38. Ito T, Hearne LJ, Cole MW (2020) **A cortical hierarchy of localized and distributed processes revealed via dissociation of task activations, connectivity changes, and intrinsic timescales** *NeuroImage* **221**
39. Jenkinson M, Bannister P, Brady M, Smith S (2002) **Improved optimization for the robust and accurate linear registration and motion correction of brain images** *Neuroimage* **17**:825–841
40. Jenkinson M, Beckmann CF, Behrens TE, Woolrich MW, Smith SM (2012) **Fsl** *Neuroimage* **62**:782–790
41. Ji JL, Spronk M, Kulkarni K, Repovš G, Anticevic A, Cole MW (2019) **Mapping the human brain’s cortical-subcortical functional network organization** *Neuroimage* **185**:35–57
42. Jovicich J *et al.* (2006) **Reliability in multi-site structural MRI studies: effects of gradient non-linearity correction on phantom and human data** *Neuroimage* **30**:436–443
43. Van der Kouwe AJ, Benner T, Salat DH, Fischl B (2008) **Brain morphometry with multiecho MPAGE** *Neuroimage* **40**:559–569
44. Kriegstein A, Noctor S, Martínez-Cerdeño V (2006) **Patterns of neural stem and progenitor cell division may underlie evolutionary cortical expansion** *Nature Reviews Neuroscience* **7**:883–890
45. Krubitzer L (2007) **The magnificent compromise: cortical field evolution in mammals** *Neuron* **56**:201–208
46. de Lange SC, Ardesch DJ, van den Heuvel MP (2019) **Connection strength of the macaque connectome augments topological and functional network attributes** *Network Neuroscience* **3**:1051–1069
47. Lecouvet F, Richard FO, Berg BV, Malghem J, Maldague B, Jamart J, Ferrant A, Michaux JL. (1997) **Long-term effects of localized spinal radiation therapy on vertebral fractures and focal lesions appearance in patients with multiple myeloma** *British journal of haematology* **96**:743–745
48. Llinás RR (2002) **I of the vortex: From neurons to self**
49. Maingault S, Tzourio-Mazoyer N, Mazoyer B, Crivello F (2016) **Regional correlations between cortical thickness and surface area asymmetries: A surface-based morphometry study of 250 adults** *Neuropsychologia* **93**:350–364

50. Mantini D *et al.* (2011) **Default mode of brain function in monkeys** *Journal of Neuroscience* **31**:12954–12962
51. Meng Y, Li G, Lin W, Gilmore JH, Shen D (2014) **Spatial distribution and longitudinal development of deep cortical sulcal landmarks in infants** *Neuroimage* **100**:206–218
52. Modha DS, Singh R (2010) **Network architecture of the long-distance pathways in the macaque brain** *Proceedings of the National Academy of Sciences* **107**:13485–13490
53. Montgomery SH (2013) **The human frontal lobes: not relatively large but still disproportionately important? A commentary on Barton and Venditti** *Brain, behavior and evolution* **82**:147–149
54. Montgomery SH, Mundy NI, Barton RA (2016) **Brain evolution and development: adaptation, allometry and constraint** *Proceedings of the Royal Society B: Biological Sciences* **283**
55. Parvizi J, Van Hoesen GW, Buckwalter J, Damasio A (2006) **Neural connections of the posteromedial cortex in the macaque** *Proceedings of the National Academy of Sciences* **103**:1563–1568
56. Patel GH, Yang D, Jamerson EC, Snyder LH, Corbetta M, Ferrera VP (2015) **Functional evolution of new and expanded attention networks in humans** *Proceedings of the National Academy of Sciences* **112**:9454–9459
57. Rettmann ME, Han X, Xu C, Prince JL (2002) **Automated sulcal segmentation using watersheds on the cortical surface** *NeuroImage* **15**:329–344
58. Rilling JK. (2006) **Human and nonhuman primate brains: are they allometrically scaled versions of the same design?** *Evolutionary Anthropology: Issues, News, and Reviews: Issues, News, and Reviews* **15**:65–77
59. Rilling JK (2014) **Comparative primate neuroimaging: insights into human brain evolution** *Trends in cognitive sciences* **18**:46–55
60. Robinson EC *et al.* (2018) **Multimodal surface matching with higher-order smoothness constraints** *Neuroimage* **167**:453–465
61. Robinson EC, Jbabdi S, Glasser MF, Andersson J, Burgess GC, Harms MP, Smith SM, Van Essen DC, Jenkinson M (2014) **MSM: a new flexible framework for multimodal surface matching** *Neuroimage* **100**:414–426
62. Rolls ET, Grabenhorst F (2008) **The orbitofrontal cortex and beyond: from affect to decision-making** *Progress in neurobiology* **86**:216–244
63. Rubinov M, Sporns O (2010) **Complex network measures of brain connectivity: uses and interpretations** *Neuroimage* **52**:1059–1069
64. Schmitt JE, Raznahan A, Liu S, Neale MC (2021) **The heritability of cortical folding: Evidence from the human connectome project** *Cerebral Cortex* **31**:702–715
65. Ségonne F, Grimson E, Fischl B. (2005) **A genetic algorithm for the topology correction of cortical surfaces. In: Information Processing in Medical Imaging: 19th International Conference, IPMI 2005, Glenwood Springs, CO, USA, July 10-15, 2005. Proceedings 19** :393–405

66. Seidlitz J, Sponheim C, Glen D, Frank QY, Saleem KS, Leopold DA, Ungerleider L, Messinger A (2018) **A population MRI brain template and analysis tools for the macaque** *Neuroimage* **170**:121–131
67. Semendeferi K, Lu A, Schenker N, Damásio H (2002) **Humans and great apes share a large frontal cortex** *Nature neuroscience* **5**:272–276
68. Sereno MI, Dale A, Reppas J, Kwong K, Belliveau J, Brady T, Rosen B, Tootell R (1995) **Borders of multiple visual areas in humans revealed by functional magnetic resonance imaging** *Science* **268**:889–893
69. Sereno MI, Tootell RB (2005) **From monkeys to humans: what do we now know about brain homologies?** *Current opinion in neurobiology* **15**:135–144
70. Smith LI (2002) **A tutorial on principal components analysis**
71. Sousa AP, Piñon MCG, Gattass R, Rosa MG (1991) **Topographic organization of cortical input to striate cortex in the Cebus monkey: a fluorescent tracer study** *Journal of comparative neurology* **308**:665–682
72. Sporns O, Zwi JD (2004) **The small world of the cerebral cortex** *Neuroinformatics* **2**:145–162
73. Teissier A, Pierani A. (2021) **Wiring of higher-order cortical areas: Spatiotemporal development of cortical hierarchy** *Seminars in Cell & Developmental Biology* :35–49
74. Tournier JD, Smith R, Raffelt D, Tabbara R, Dhollander T, Pietsch M, Christiaens D, Jeurissen B, Yeh CH, Connelly A. (2019) **MRtrix3: A fast, flexible and open software framework for medical image processing and visualisation** *Neuroimage* **202**
75. Van Essen DC, Dierker DL (2007) **Surface-based and probabilistic atlases of primate cerebral cortex** *Neuron* **56**:209–225
76. Van Essen DC, Donahue CJ, Coalson TS, Kennedy H, Hayashi T, Glasser MF (2019) **Cerebral cortical folding, parcellation, and connectivity in humans, nonhuman primates, and mice** *Proceedings of the National Academy of Sciences* **116**:26173–26180
77. Van Essen DC, Donahue CJ, Glasser MF (2018) **Development and evolution of cerebral and cerebellar cortex** *Brain, behavior and evolution* **91**:158–169
78. Van Essen DC, Glasser MF, Dierker DL, Harwell J (2012) **Cortical parcellations of the macaque monkey analyzed on surface-based atlases** *Cerebral cortex* **22**:2227–2240
79. Van Essen DC *et al.* (2012) **The Human Connectome Project: a data acquisition perspective** *Neuroimage* **62**:2222–2231
80. Varriano F, Pascual-Diaz S, Prats-Galino A (2018) **When the FAT goes wide: Right extended Frontal Aslant Tract volume predicts performance on working memory tasks in healthy humans** *PLoS One* **13**
81. Vincent JL, Patel GH, Fox MD, Snyder AZ, Baker JT, Van Essen DC, Zempel JM, Snyder LH, Corbetta M, Raichle ME (2007) **Intrinsic functional architecture in the anaesthetized monkey brain** *Nature* **447**:83–86

82. White L, Andrews T, Hulette C, Richards A, Groelle M, Paydarfar J, Purves D. (1997) **Structure of the human sensorimotor system. I: Morphology and cytoarchitecture of the central sulcus** (*J Neurosci* **17**:18–30)
83. Whittle S, Allen NB, Fornito A, Lubman DI, Simmons JG, Pantelis C, Yücel M (2009) **Variations in cortical folding patterns are related to individual differences in temperament** *Psychiatry Research: Neuroimaging* **172**:68–74
84. Willemet R (2015) **Commentary: Greater addition of neurons to the olfactory bulb than to the cerebral cortex of eulipotyphlans but not rodents, afrotherians or primates** *Frontiers in neuroanatomy* **9**
85. Xu T *et al.* (2020) **Cross-species functional alignment reveals evolutionary hierarchy within the connectome** *Neuroimage* **223**
86. Yan W, Fan J, Zhang X, Song H, Wan R, Wang W, Yin Y (2021) **Decreased neuronal synaptosome associated protein 29 contributes to poststroke cognitive impairment by disrupting presynaptic maintenance** *Theranostics* **11**
87. Yang F, Kruggel F (2008) **Automatic segmentation of human brain sulci** *Medical image analysis* **12**:442–451
88. Yang S *et al.* (2019) **Temporal variability of cortical gyral-sulcal resting state functional activity correlates with fluid intelligence** *Frontiers in neural circuits* **13**
89. Yang Z, Qiu J, Wang P, Liu R, Zuo XN (2016) **Brain structure–function associations identified in large-scale neuroimaging data** *Brain Structure and Function* **221**:4459–4474
90. Zhang S *et al.* (2022) **Gyral peaks: Novel gyral landmarks in developing macaque brains** *Human Brain Mapping* **43**:4540–4555
91. Zhang S, Zhang T, He Z, Li X, Zhang L, Zhu D, Jiang X, Liu T, Han J, Guo L (2023) **Gyral peaks and patterns in human brains** *Cerebral Cortex*

Article and author information

Songyao Zhang

School of Automation, Northwestern Polytechnical University, Xi'an, China

Tuo Zhang

School of Automation, Northwestern Polytechnical University, Xi'an, China

For correspondence: tuo Zhang@nwpu.edu.cn

Guannan Cao

School of Automation, Northwestern Polytechnical University, Xi'an, China

Jingchao Zhou

College of Science, North China University of Science and Technology, Tangshan, China

Zhibin He

School of Automation, Northwestern Polytechnical University, Xi'an, China

Xiao Li

School of Information Technology, Northwest University, Xi'an, China

Yudan Ren

School of Information Technology, Northwest University, Xi'an, China

Tao Liu

College of Science, North China University of Science and Technology, Tangshan, China

Xi Jiang

School of Life Science and Technology, MOE Key Lab for Neuroinformation, University of Electronic Science and Technology of China, Chengdu, China

Lei Guo

School of Automation, Northwestern Polytechnical University, Xi'an, China

Junwei Han

School of Automation, Northwestern Polytechnical University, Xi'an, China

Tianming Liu

Cortical Architecture Imaging and Discovery Lab, Department of Computer Science and Bioimaging Research Center, University of Georgia, Athens, GA, USA

Copyright

© 2023, Zhang et al.

This article is distributed under the terms of the [Creative Commons Attribution License](#), which permits unrestricted use and redistribution provided that the original author and source are credited.

Editors

Reviewing Editor

Andre Marquand

Radboud University Nijmegen, Nijmegen, Netherlands

Senior Editor

Jonathan Roiser

University College London, London, United Kingdom

Reviewer #1 (Public Review):

Zhang et al. tackle the important topic of primate-specific structural features of the brain and the link with functional specialization. The authors explore and compare gyral peaks of the human and macaque cortex through non-invasive neuroimaging, using convincing techniques that have been previously validated elsewhere. They show that nearly 60% of the macaque peaks are shared with humans, and use a multi-modal parcellation scheme to describe the spatial distribution of shared and unique gyral peaks in both species.

The claim is made that shared peaks are mainly located in lower-order cortical areas whereas unique peaks are located in higher-order regions, however, no systematic

comparison is made. The authors then show that shared peaks are more consistently found across individuals than unique peaks, and show a positive but small and non-significant correlation between cross-individual counts of the shared peaks of the human and the macaque i.e. the authors show a non-significant trend for shared peaks that are more consistently found across humans to be those that are also more found across macaques.

In order to identify if unique and shared peaks could be identified based on the structural features of the cortical regions containing them, the authors compared them with t-tests. A correction for multiple comparisons should be applied and t-values reported. Graph-theoretical measures were applied to functional connectivity datasets (resting-state fMRI) and compared between unique and shared peak regions for each species separately. Again the absence of multiple comparison correction and t-values make the results hard to interpret. The same comment applies to the analysis reporting that shared peaks are surrounded by a larger number of brain regions than unique peaks. Finally, the potentially extremely interesting results about differential human gene expression of shared and unique peaks regions are not systematically reported e.g. the 28 genes identified are not listed and the selection procedure of 7 genes is not fully reported.

The paper is well written and the methods used for data processing are very compelling i.e. the peak cluster extraction pipeline and cross-species registration.

Comments on revision:

The authors have convincingly addressed all my previous concerns such that, as the revised paper stands now, the presented results provide solid support for the conclusions of the authors. The revised paper is now of interest for a large part of the neuroscience community and specifically for those interested in primate-specific structural features of the brain and the link with functional specialization.

<https://doi.org/10.7554/eLife.90182.2.sa0>

Author Response

The following is the authors' response to the original reviews.

Public review

Reviewer 1

Zhang et al. tackle the important topic of primate-specific structural features of the brain and the link with functional specialization. The authors explore and compare gyral peaks of the human and macaque cortex through non-invasive neuroimaging, using convincing techniques that have been previously validated elsewhere. They show that nearly 60% of the macaque peaks are shared with humans, and use a multi-modal parcellation scheme to describe the spatial distribution of shared and unique gyral peaks in both species.

We thank the reviewer for his/her summary and affirmation of our work.

The claim is made that shared peaks are mainly located in lower-order cortical areas whereas unique peaks are located in higher-order regions, however, no systematic comparison is made. The authors then show that shared peaks are more consistently found across individuals than unique peaks, and show a positive but small and non-significant correlation between cross-individual counts of the shared peaks of the human and the macaque i.e. the authors show a non-significant trend for shared peaks that are

more consistently found across humans to be those that are also more found across macaques.

Answer: We appreciate the reviewer for raising questions about our work. In order to provide a more systematic comparison for the conclusion that ‘shared peaks are mainly located in lower-order cortical areas whereas unique peaks are located in higher-order regions’, we have conducted two additional experiments. Following the reviewers’ suggestions, we conducted a statistical analysis of the ratio of shared and unique peaks within different brain networks (as depicted in Figure 2 (b)), and also presented the specific distribution quantities of the two types of peaks in both low- and high-order brain networks (as detailed in the corresponding Table 1). Through these three experiments, we have obtained a more systematic and comprehensive conclusion that ‘shared peaks are more distributed in lower-order networks, while unique peaks are more in higher-order networks’.

In order to identify if unique and shared peaks could be identified based on the structural features of the cortical regions containing them, the authors compared them with t-tests. A correction for multiple comparisons should be applied and t-values reported. Graph-theoretical measures were applied to functional connectivity datasets (resting-state fMRI) and compared between unique and shared peak regions for each species separately. Again the absence of multiple comparison correction and t-values make the results hard to interpret. The same comment applies to the analysis reporting that shared peaks are surrounded by a larger number of brain regions than unique peaks. Finally, the potentially extremely interesting results about differential human gene expression of shared and unique peaks regions are not systematically reported e.g. the 28 genes identified are not listed and the selection procedure of 7 genes is not fully reported.

Answer: We appreciate the reviewer for their suggestions about the statistical analysis in our manuscript. Firstly, we applied False Discovery Rate (FDR) correction to all experiments involving multiple comparisons throughout the entire manuscript, and the corrected t-values are reported (Table 2-5 and A5-A6). Additionally, in response to the reviewers’ guidance regarding the gene analysis section, we provided a list of 28 genes (Table A7) selected by lasso, along with the t-values obtained from Welch’s t-test for the expression of the two type of peaks. The functions corresponding to the seven genes with final t-values below 0.05 are reported in Table 6.

The paper is well written and the methods used for data processing are very compelling i.e. the peak cluster extraction pipeline and cross-species registration. However, the analysis and especially the reporting of statistics, as they stand now, constitutes the main weakness of the paper. Some aspects of the statistical analysis need to be clarified.

Reviewer 2

The authors compared the cortical folding of human brains with folding in macaque monkey brains to reveal shared and unique locations of gyral peaks. The shared gyral peaks were located in cortical regions that are functionally similar and less changed in humans from those in macaques, while the locations of unique peaks in humans are in regions that have changed or expanded functions. These findings are important in that they suggest where human brains have changed more than macaque brains in their subsequent evolution from a common ancestor. The massive analysis of comparative results provides evidence of where humans and macaques are similar or different in cortical markers, as well as noting some of the variations within each of the two primates.

Answer: Gratitude to the reviewer for his/her summary and appreciation of our cross-species work.

Strengths:

The study includes massive detail.

Weaknesses:

The manuscript is too long and there is not enough focus on the main points.

Answer: We appreciate the reviewer for pointing out the shortcomings in our manuscript. Firstly, considering the manuscript is too long, we have chosen to retain only the core experiments and relevant analyses in the main text. Relatively minor conclusions have been moved to the supplementary information, such as original Table 1 is now moved to the Supplementary Information as Table A1 (locations of all shared clusters). Additionally, some non-essential expressions in the original manuscript have been removed.

Our experiments primarily revealed the existence of partially shared cortical landmarks, known as gyral peaks, in both humans and macaques. We found that these shared and unique peaks are mainly distributed across low- and high-order brain networks. To emphasize this main point, we added two experiments on top of the existing ones to provide a more systematic explanation of this conclusion. We conducted a statistical analysis of the ratio of shared and unique peaks within different brain networks (as depicted in Figure 2 (b)), and also presented the specific distribution quantities of the two types of peaks in both low- and high-order brain networks (as detailed in the corresponding Table 1). By combining the results of these two experiments with the original manuscript's statistical findings on the proportions of the two type of peaks in different brain networks, the conclusion that 'shared and unique peaks are predominantly located in low-order and high-order brain networks' becomes more prominent.

A brief listing of previous views on why fissures form and what factors are important would be helpful.

Answer: In response to this suggestion from the reviewer, we have incorporated some previous views on why fissures form and what factors are important into the 'Introduction' section.

'Cortical folds are important features of primate brains. The primary driver of cortical folding is the differential growth between cortical and subcortical layers. During the gyrification process in the cortex, areas with high-density stiff axonal fiber bundles towards gyri. The brain's folding pattern formed through a series of complex processes. The folding patterns in the brain, formed through a series of complex processes, are found to play a crucial role in various cognitive and behavioral processes, including perception, action, and cognition (Fornito et al. 2004; Cachia et al. 2018; Yang et al. 2019; Whittle et al. 2009).'

Reviewer 1 (Recommendations For The Authors):

(1) Figure 3b shows a non-significant trend for shared peaks that are more consistently found across humans to be those that are also more found across macaques. In the discussion, lines 218-219, the fact that the correlation is not significant should be reported more clearly.

Answers: We thank the reviewer for this question. We revised the Line 218-219 (now Line 257-259) as follows: '2. Consistency: The inter-individual consistency of shared peaks within

each species was greater than that of unique peaks. The consistency of shared peaks in the human and macaque brains exhibits a positive correlation (non-significant though).’

(2) It is not fully clear how much shared peaks are mostly distributed in the higher-order cortex, especially in the macaque. It is reported in the results lines 132-133 that ‘In the macaque brain, shared peak cluster centers most distributed in the V2, DMN, and CON (Figure.2 (d)), while unique peak cluster centers most distributed in the DMN, Language (Lan), and Dorsal-attention (DAN)’ but not further discussed. Please develop this point in the discussion. Further, the results presented in Figures 2 and A1 are actually quite different and this shall be better described in the results. Given that shared and unique peaks can be found in the same region, this analysis would gain importance by applying a comparison test for the selection of regions where the most shared or unique peaks are found. The sentence lines 306-308 should be accordingly revised.

It is hard to understand what the 0-3% corresponds to in Figures 2 and A1?

Please also correct in both legends and in the text the labeling of panels and add in the legends a brief description of panel (c). In the legend of Figure 2, ‘shared peaks’ in the second sentence shall be replaced by ‘unique peaks’.

Answers: We thank the reviewer for these questions and suggestions. Our responses to them are itemized as follows:

A1: In general, to clarify the distribution of shared and unique peaks in the high-order and low-order networks, we divided 12 brain networks in Cole-Anticevic atlas into the low-order networks (visual 1 (V1), visual 2 (V2), auditory (Aud), somatomotor (SMN), posterior multimodal (PMN), ventral multimodal (VMN), and orbito-affective networks (OAN)) and higher-order networks (include cingulo-opercular (CON), dorsal attention (DAN), language (Lan), frontoparietal (FPN), default mode network (DMN)) based on previous research (Golesorkhi et al. 2022; Ito, Hearne, and Cole 2020). On this lower/higher -order division, we reported the number of shared and unique peaks in both species in Author response table 1. It is found that, whether in humans or macaques, shared peaks are more distributed in lower-order networks, while unique peaks are more in higher-order networks. This observation is particularly pronounced in humans.

Author response table 1.

The number of shared and unique peaks in lower- and higher-order brain networks of the two species. Lower-order networks include visual 1 (V1), visual 2 (V2), auditory (Aud), somatomotor (SMN), posterior multimodal (PMN), ventral multimodal (VMN), and orbito-affective networks (OAN), higher-order networks include cingulo-opercular (CON), dorsal attention (DAN), language (Lan), frontoparietal (FPN), default-mode network (DMN).

Lower/Higher networks	Human	Macaque
Shared peak	33/18	29/22
Unique peak	37/104	14/20

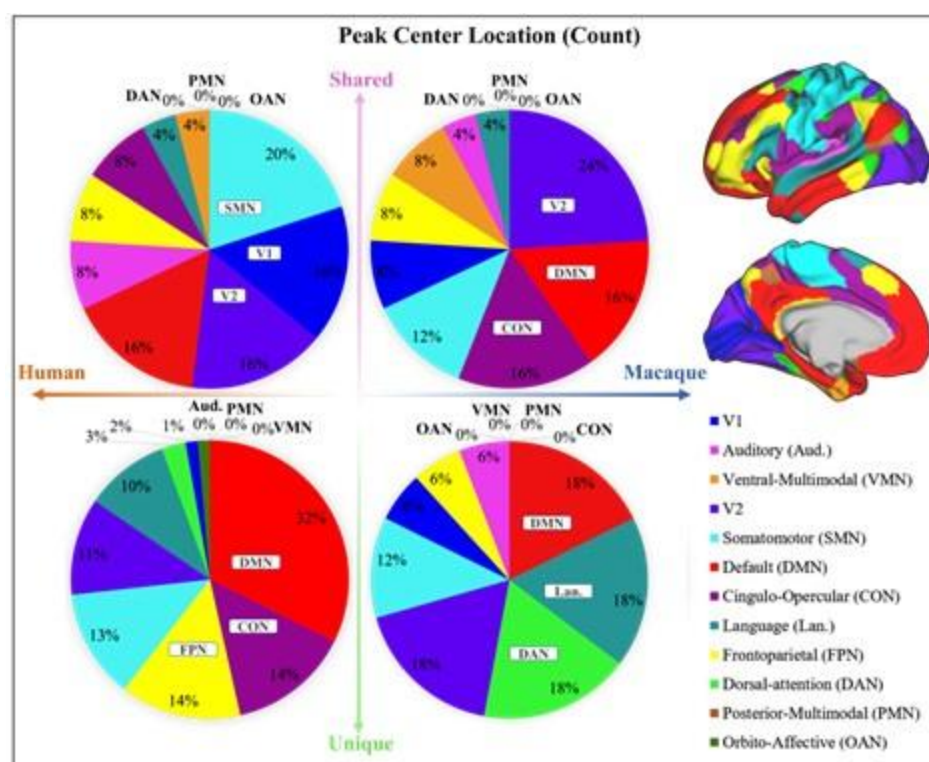
In the main text, Figure 2 (referring to Author response figure 1 later in the text.) illustrates the proportions of shared and unique peaks across 12 brain networks in both species. In each pie chart, we have specifically highlighted the top three ranked brain regions. Although the

pie chart also generally supports the above results, two brain networks deserve further discussion. They are DMN and CON, two higher-order networks that have higher ranks in terms of shared peak count (the second-ranked and the third-ranked on macaque shared peaks; the fourth-ranked and the fifth-ranked on human shared peaks).

The cingulo-opercular network (CON) is a brain network associated with action, goal, arousal, and pain. However, a study found three newly discovered areas of the primary motor cortex that exhibit strong functional connectivity with the CON region, forming a novel network known as the somato-cognitive action network (SCAN) (Gordon et al. 2023). The SCAN integrates body control (motor and autonomic) and action planning, consistent with the findings that aspects of higher-level executive control might derive from movement coordination (Llinás 2002; Gordon et al. 2023). CON may be shared in the form of the SCAN network across these two species. This could explain in part the results in Author response figure 1 that shared peaks are more on CONs.

Author response image 1.

Pie chart shows the count of shared and unique peaks across different brain networks for both human and macaque. Right panel shows the Cole-Anticevic (CA) networks (Ji et al. 2019) on human surface as a reference.



Default-mode network (DMN) is a ensemble of brain regions that are active in passive tasks, including the anterior and posterior cingulate cortex, medial and lateral parietal cortex, and medial prefrontal cortex (Buckner, Andrews-Hanna, and Schacter 2008). Although DMN is considered a higher-order brain network, numerous studies have provided evidence of its homologous presence in both humans and macaques. Many existing studies have confirmed the similarity between the DMN regions in humans and macaques from various perspectives, including cytoarchitectonic (Parvizi et al. 2006; Buckner, Andrews-Hanna, and Schacter 2008; Caminiti et al. 2010) and anatomical tracing (Vincent et al. 2007). These studies all support the notion that some elements of the DMN may be conserved across primate species (Mantini et

al. 2011). In general, the partial sharing of DMN between humans and macaques may be attributed to the higher occurrence of shared peaks within the DMN.

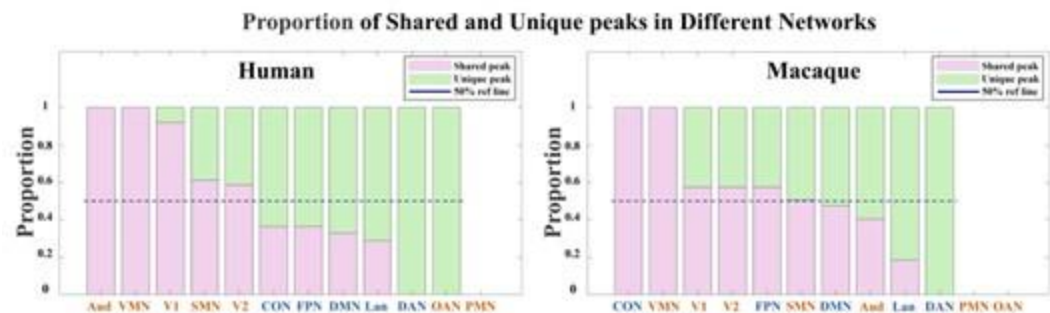
These results have been added to Table 2 along with corresponding text and discussion section.

A2: The difference between the results of Figure 2 and Figure A1 (now Figure A2) is whether the peak count is normalized by cortical area, which hugely varies across networks. For example, among the 12 brain networks, the three networks with the largest surface areas are the DMN, SMN and CON, and the three networks with the smallest area are OAN, PMN and VMN. The area difference between networks can be as large as 18-fold. Therefore, it is not difficult to find that, although the DMN ranks high in both shared and unique peak counts during statistical analysis (Figure 2 (a)), it is relatively small in Figure A2 after area normalization. In contrast, VMN ranks lower in peak count statistics but exhibits a substantial proportion after area normalization (For example, 38% of macaque shared peaks are distributed in the VMN region, but there are actually only four peaks). However, the two pie charts deliver the same message that there are more shared peaks in lower-order networks, while unique peaks are more in higher-order networks (except for macaques, where shared peaks are also distributed significantly in DMN and CON).

Following the suggestion from the reviewer, we adopted a new approach to present the ratio between shared peak count and unique peak count for each network (see Author response figure 2), such that the networks where the most shared or unique peaks are found can be easily highlighted. To mitigate potential imbalances in proportions caused by differences in the absolute numbers of each category (shared or unique) of peak, the proportions of peaks within their respective categories were utilized in the calculations. In Author response figure 2, the pink and green color bins represent ratios of shared and unique peaks, respectively. The dark blue dashed line represents the 50% reference line. In general, from left to right in the figure, the ratio of shared peaks decreases gradually while the ratio of unique peaks increases, suggesting that shared peaks are more (>0.5 , above the dashed line) on lower-order networks (orange font), while unique peaks are generally more on higher-order networks (blue font). In specific, in human brains, the networks with a higher abundance of shared peaks are Aud, VMN, V1, SMN, and V2; whereas in macaques, they are CON, VMN, V1, V2, FPN, and SMN. Again, in the human brains, the disparity between shared and unique peaks tends to be more significant (further away from the reference line), for both lower-order and higher-order networks, respectively. In contrast, in the macaque brains, the disparity between shared and unique peaks is less significant (closer to the reference line). The ratio of shared and unique peaks is around 0.5 for 6 out of all 10 networks (including both lower and higher-order ones).

Author response image 2.

The ratio of shared and unique peaks in each brain network in the Cole-Anticevic (CA) atlas. The pink and green color bins represent ratios of shared and unique peaks, respectively. The dark blue dashed line represents the 50% reference line. For each brain region, the sum of the ratios of shared and unique peaks is equal to 1.



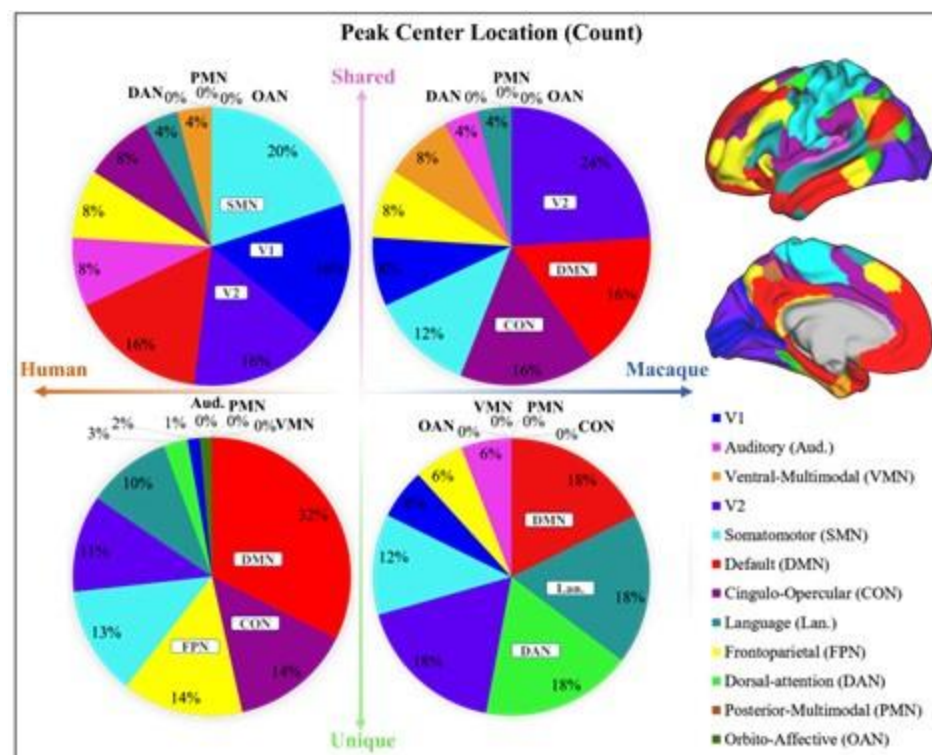
Based on these analyses, the sentence lines 306-308 (now Line 368-370) has been revised as follows: ‘In the human brain, the more shared peaks (about 65%) are located in lower-order brain regions, while unique peaks are mainly (about 74%) located in higher-order regions. However, this trend is relatively less pronounced in the macaque brain.’

These results have been added to Figure 2 (b) along with corresponding text and discussion section.

A3: In response to the third suggestion from the reviewer, we have clearly labeled the brain region names corresponding to 0% to 3% in Figure 2 (now Figure 2 (a)) and Figure A1 (now Figure A2).

Author response image 3.

Pie chart shows the count of shared and unique peaks across different brain networks for both human and macaque. Right panel shows the Cole-Anticevic (CA) networks (Ji et al. 2019) on human surface as a reference.



A4: Finally, we would like to express our gratitude to the reviewer for pointing out our mistakes.

We have made improvements to Figure 2 and revised the figure captions accordingly.

(3) The conclusions regarding the spatial relationship between peaks and functional regions shall be revised (Lines 187-188, 228-229, and 329-330). In the macaque, the results are opposite in the two atlases used. Further, in the human, it is not clear how multiple comparison corrections will impact statistics and some atlases show opposite results, although conclusions hold true in the majority of human atlases.

Answers: We thank the reviewer very much for this suggestion. We have added the results of the Cole-Anticevic atlas for macaques in the main text, which also has the observation that shared > unique (Author response table 2, corresponds to Table 5 in main text), namely, there are more diverse brain regions around shared peaks than around unique peaks. Therefore, out of the commonly used three macaque atlases, two (Markov91 and Cole-Anticevic) conform to this observation, while BA05 does not. We utilized false discovery rate (FDR) correction for multiple comparisons, and the corrected p-values are reported in Tables (in the revised main text and are shown below). Results on atlas with multiple resolutions are reported in Author response table 4) (Table A6 in the Supplementary Information). The observation that more diverse brain regions around shared peaks than around unique peaks, holds for human atlases in Author response table 3) (Table 4 in main text), where the atlas resolutions ranges from 7 parcels to 300 parcels, demonstrating the robustness of the conclusion. It is noted that the observation is not consistent on atlases with relatively lower resolutions (e.g., BA05 for macaque, $n=30$ and Yeo2011 for human, $n=7$) or, in particular, higher resolutions (e.g., Schaefer-500, and Vosdewael-400, $n>300$). This inconsistency could be reasonable since the resolution of the parcellation itself will largely determines the chance of a cortical region appear in a peak's neighborhood, if the parcellation is too coarse or too fine. For example, if $n=1$ (the entire cortex is the only one region) or $n=30k$ (each vertex is a region), each peak will has the same number of neighboring regions for these two extreme cases (one brain region for each peak for $n=1$; around 30 vertices for each peak for $n=30k$).

In conclusion, we observed that there are more diverse brain regions around shared peaks than around unique peaks for multiple brain atlases with a median parcellation resolution. These results have been added to Tables 4, 5, and A6 along with corresponding text and discussion section.

Author response table 2.

The mean values (\pm SD) of brain regions that appeared within a 3-ring neighborhood for shared and unique peaks in 3 common macaque atlases. For both Markov91 and Cole-Anticevic atlas, the shared peaks has more variety of functional regions around it than the unique peaks. But for the atlas BA05, the conclusion was reversed. The bold font represent the larger values between the shared peak and unique peaks. All $p<0.001$, after false discovery rate (FDR) corrected.

Atlas Name	Markov91	Cole-Anticevic	BA05
Share	2.73±0.27	1.77±0.17	1.61±0.16
Nbr Unique Nbr	2.16±0.15	1.58±0.16	1.80±0.16
p	<0.001	<0.001	<0.001
t	-7.4	14.93	6.49

(4) For Tables 2-4, A4, and Figure 3a, please indicate in all the legends if values correspond to Mean plus minus Standard Deviation, report t-value, and n in the legend or in the text.

Answers: We thank the reviewer very much for this suggestion. We added the ‘mean (±SD)’ in the notes of Tables 2-4, A4 (now A6), and Figure 3 (a). All the t and n values of t-test are reported in tables or in the main text.

(5) Please create a statistical section in the Methods to describe more precisely the tests used e.g. for t-tests, if datasets follow a normal distribution with unknown variance. In the case of multiple comparisons like in e.g. Table 2-4, A4, please report what multiple comparisons correction was used to adjust the significance level.

Author response table 3.

The mean values (±SD) of brain regions that appeared within a 3-ring neighborhood for shared and unique peaks in 10 common human atlases. All the shared peaks in the table have a greater number of neighboring brain regions compared to the unique peaks. All $p < 0.001$, false discovery rate (FDR) corrected.

Atlas Name	Glasser2016	Schaefer-100	Schaefer-200	Schaefer-300	Vosdewael-100
Share Nbr	2.43±0.15	1.89±0.12	2.12±0.11	2.23±0.11	1.57±0.17
Unique Nbr	2.37±0.09	1.74±0.09	2.08±0.10	2.17±0.10	1.46±0.10
p	<0.001	<0.001	<0.001	<0.001	<0.001
t	8.32	26.66	4.50	18.08	34.09
Atlas Name	Yeo2011(17)	Aparc	Aparc2009	BA	Cole-Anticevic
Share Nbr	1.76±0.11	1.58±0.12	1.95±0.13	1.58±0.12	1.65±0.11
Unique Nbr	1.73±0.08	1.33±0.07	1.94±0.09	1.29±0.08	1.57±0.07
p	<0.001	<0.001	<0.001	<0.001	<0.001
t	22.29	56.37	3.80	69.84	22.44

Author response table 4.

The mean values (±SD) of brain regions where shared and unique peaks appeared within a 3-ring neighborhood in 21 common human atlases. The p-values were corrected by FDR.

Atlas Name	Yeo2011 (7)	Glasser2016	Schaefer-100	Schaefer-200	Schaefer-300	Schaefer-400	Schaefer-500
Share Nbr	1.48±0.10	2.43±0.15	1.89±0.12	2.12±0.11	2.23±0.11	2.46±0.13	2.50±0.14
Unique Nbr	1.54±0.07	2.37±0.09	1.74±0.09	2.08±0.10	2.17±0.10	2.39±0.09	2.51±0.09
p-t	<0.001 -8.04	<0.001 8.32	<0.001 26.66	<0.001 4.50	<0.001 18.08	<0.001 17.60	<0.001 7.72
Atlas Name	Schaefer-600	Schaefer-700	Schaefer-800	Schaefer-900	Schaefer-1000	Vosdewael-100	Vosdewael-200
Share Nbr	2.48±0.14	2.76±0.14	2.85±0.16	2.86±0.12	3.07±0.14	1.57±0.17	1.71±0.11
Unique Nbr	2.60±0.10	2.74±0.10	2.74±0.12	2.87±0.09	3.03±0.10	1.46±0.10	1.73±0.08
p-t	<0.001 -14.04	0.39 2.42	<0.001 11.98	<0.001 -5.75	<0.001 4.23	<0.001 34.09	<0.001 7.44
Atlas Name	Vosdewael-300	Vosdewael-400	Yeo2011(17)	Aparc	Aparc2009	BA	Cole-Anticevic
Share Nbr	1.96±0.12	2.21±0.15	1.76±0.11	1.58±0.12	1.95±0.13	1.58±0.12	1.65±0.11
Unique Nbr	2.02±0.09	2.32±0.10	1.73±0.08	1.33±0.07	1.94±0.09	1.29±0.08	1.57±0.07
p-t	<0.001 5.41	0.13 -2.82	<0.001 22.29	<0.001 56.37	<0.001 3.80	<0.001 69.84	<0.001 22.44

Answers: Thanks for the reviewer's suggestion, we added a 'Statistic Analysis' section in the 'Materials and Methods' part:

'All variables used in the two-samples t-test follow a normal distribution check and all p-values were corrected for multiple comparisons using the false discovery rate (FDR) method. Moreover, in order to identify differently expressed genes between shared and unique peaks, we employed the Welch's t-test, given the unequal sample sizes for shared and unique peaks. For all tests, a p-value <0.05 was considered significant (FDR corrected).'

For the experiments of multiple comparisons such as Table 2-4, A4 (now A6), etc., we have added explanations in the main text, multiple comparisons correction has been corrected by false discovery rate (FDR), p-value<0.05 is considered significant.

(6) It would be of great interest to provide the full list of the 28 genes that significantly contributed to the classification of shared and unique peaks. Please provide a description of the Welch's t-test results. From the 7 genes selected, only two are discussed. Could the authors please describe briefly the function of the other genes? Although we understand that they are not associated with neuronal activity and brain function.

Answers: We thank the reviewer for these suggestions. We have provided a complete list of 28 genes selected by LASSO in the Author response table 5. Additionally, Welch's t-test was employed to calculate p-values for the expression differences of each gene in shared and unique peak clusters, and the results are also reported in the Author response table 5.

Author response table 5.

The 28 genes selected by LASSO and their corresponding p-values from Welch's t-test.

Gene Symbol	p	Gene Symbol	p	Gene Symbol	p	Gene Symbol	p
INPP4A	0.76	TLR1	0.02	KCNH5	0.04	OTULIN	0.18
ITGA1	0.19	TPST1	0.94	TMEM248	0.27	DTX2	0.15
JUNB	0.57	SNAP29	0.01	ANO2	0.26	SERPINB9P1	0.12
PECAM1	0.04	TRAM2	0.70	PLEKHA3	0.90	LHFPL5	0.63
PRKCH	0.10	DHRS4	0.05	PLBD1	0.01	GK5	0.51
NECTIN1	0.84	LPIN1	0.34	DENND1C	0.37	ZNF662	0.77
SRC	0.20	BHMT2	0.01	CXXC4	0.20	NAP1L6	0.58

Seven genes showed significant differential expression between shared and unique peaks in Welch's t-test. These genes were PECAM1, TLR1, SNAP29, DHRS4, BHMT2, PLBD1, KCNH5. Brief descriptions of their functions are listed in Author response table 6. All gene function descriptions were derived from the NCBI website (<https://www.ncbi.nlm.nih.gov/>).

These results have been added to Tables 6 and A7 along with corresponding text.

(6) For comparison, could the authors provide a supplementary figure of shared peak clusters like in Figure 1b but displayed on the surface of the macaque brain template?

Answers: We thank the reviewer very much for this suggestion and we have incorporated a display of shared peak clusters on the macaque brain template surface (Author response figure 4, corresponds to Figure A1 of Supplementary Information.)

(7) Could the author develop or rephrase the sentence lines 69-72 which remains unclear?

Answers: We appreciate the reviewer's feedback and have revised this sentence to ensure clarity. The sentences from line 69 to 72 have been revised to 'In the study of macaques, it has been observed that the peak consistently present across individuals is located on more curved gyri (S. Zhang, Chavoshnejad, et al. 2022). Similar conclusions have been drawn in human brain research (S. Zhang, T. Zhang, et al. 2023).' Now, this sentence corresponds to lines 74-77 in the main text.

(8) Line 99: please indicate which section.

Author response table 6.

Seven genes were selected using LASSO that showed significant differential expression in shared and unique peaks.

Gene Symbol	Gene Function
PECAM1	The protein encoded by this gene is found on the surface of platelets, monocytes, neutrophils, and some types of T-cells, and makes up a large portion of endothelial cell intercellular junctions. The encoded protein is a member of the immunoglobulin superfamily and is likely involved in leukocyte migration, angiogenesis, and integrin activation. [provided by RefSeq, May 2010]
TLR1	The protein encoded by this gene is a member of the Toll-like receptor (TLR) family which plays a fundamental role in pathogen recognition and activation of innate immunity. They recognize pathogen-associated molecular patterns (PAMPs) that are expressed on infectious agents, and mediate the production of cytokines necessary for the development of effective immunity. [provided by RefSeq, Jul 2008]
SNAP29	This gene, belonging to the SNAP25 gene family, encodes a protein involved in various membrane trafficking processes. Other members of this gene family, such as SNAP23 and SNAP25, encode proteins that bind to a syntaxin protein and facilitate the docking and fusion of synaptic vesicle membranes with the plasma membrane. [provided by RefSeq, Jul 2008]
DHRS4	Exhibits protein binding and oxidoreductase activities, involved in cellular metabolic processes including ketone metabolism, regulation of reactive oxygen species, and steroid metabolism. Found in the nucleus and peroxisomal membrane. [provided by Alliance of Genome Resources, Apr 2022]
BHMT2	Homocysteine, a sulfur-containing amino acid, is crucial for methylation reactions. The protein encoded by this gene is one of two methyltransferases that facilitate the transfer of a methyl group from betaine to homocysteine. Irregularities in homocysteine metabolism have been linked to conditions ranging from vascular disease to neural tube birth defects. This gene has alternatively spliced transcript variants encoding different isoforms.[provided by RefSeq, May 2010]
PLBD1	Predicted to enable phospholipase activity. Predicted to be involved in phospholipid catabolic process. Located in extracellular space. [provided by Alliance of Genome Resources, Apr 2022]
KCNH5	This gene encodes a member of voltage-gated potassium channels. Members of this family have diverse functions, including regulating neurotransmitter and hormone release, cardiac function, and cell volume. This protein is an outward-rectifying, noninactivating channel. Alternative splicing results in multiple transcript variants. [provided by RefSeq, Jul 2013]

Answers: We thank the reviewer very much for this suggestion and we revised this sentence to ‘The definition of peaks and the method for extracting peak clusters within each species are described in the Materials and Methods section’.

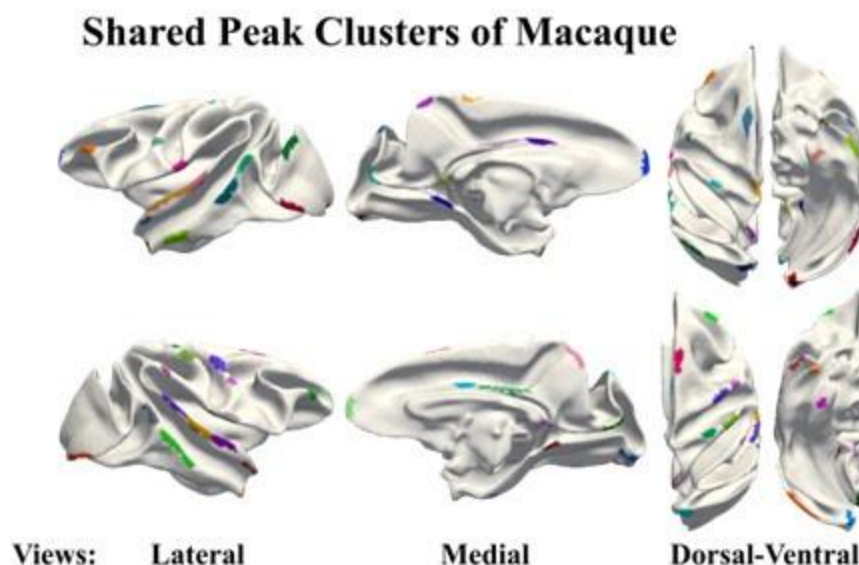
(9) In Figure 3b, please report R2 and p-value. A semi-log might be more appropriate given the overdispersion of Human Peak Counts.

Answers: We thank the reviewer very much for this suggestion. Linear regression analysis was conducted on the average counts of all corresponding shared peak clusters of human and

macaque. The horizontal and vertical axes of the Author response figure 5 (b) represent the average count of shared peaks in the macaque and human brains, respectively. The Pearson correlation coefficient (PCC) of the interspecies consistency of the left and right brain is 0.20 and 0.26 ($p > 0.05$ for both), respectively. The result of linear regression shows that there is a positive correlation in the inter-individual consistency of shared peaks between macaque and human brains, but it is not statistically significant (with R^2 for the left and right brain are 0.07 and 0.01, respectively).

Author response image 4.

Shared peak clusters of macaque, shows on macaque brain template.



The goodness of fit (R^2), pearson correlation coefficient (PCC), and their respective p-values were indicated in Author response figure 5 (b). To avoid overdispersion, the peak count of the human brain is displayed in a semi-log format.

The updated Figure and results are presented in Figure 3 of the main text.

(10) Line 177: please indicate where in the Supplementary Information.

Answers: Thank you for the reviewer's reminder. We have incorporated the results of the human brain structural connectivity matrix into Table A5 in the Supplementary Information and provided corresponding indications in the main text.

(11) Line 226: please correct 'except for betweenness [and efficiency] of the'.

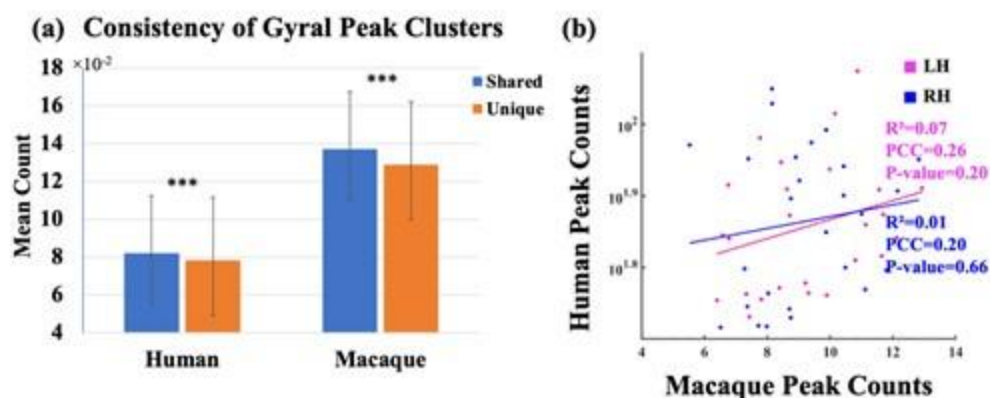
Answers: We thank the reviewer very much for this suggestion and we added 'and efficiency' in original Line 173 and 226 (now Line 206 and 267) after 'betweenness'.

(12) The gene expression dataset used is from the Allen Human Brain Atlas (AHBA). Reference to Hawrylycz et al., 2012 Nature. 2012 Sep 20;489(7416):391-399. doi: 10.1038/nature11405 shall be made and abbreviation defined at first use in the text.

Answers: We added the full name 'Allen Human Brain Atlas' when AHBA is first mentioned, along with the reference suggested by the reviewer.

Author response image 5.

(a) Mean peak count (\pm SD) covered by shared and unique peak clusters in two species. ***indicates $p < 0.001$. The t-values for the t-tests in humans and macaques are 4.74 and 2.67, respectively. (b) Linear regression results of the consistency of peak clusters shared between macaque and human brains. The pink and blue colors represent the left and right hemispheres, respectively. The results of the linear regression are depicted in the figure. While there was a positive correlation observed in the consistency of gyral peaks between macaque and human, the obtained p-value for the fitted results exceeded the significance threshold of 0.05.



(13) Line 17: remove 'are'.

Answers: We thank the reviewer very much for this suggestion and we removed 'are' in Line 17 (now Line 18).

(14) Line 201: remove 'is used'.

Answers: We thank the reviewer very much for this suggestion and we removed 'is used' in Line 201 (now Line 237).

References

Buckner, Randy L, Jessica R Andrews-Hanna, and Daniel L Schacter (2008). "The brain's default network: anatomy, function, and relevance to disease". In: Annals of the new York Academy of Sciences 1124.1, pp. 1–38.

Cachia, Arnaud et al. (2018). "How interindividual differences in brain anatomy shape reading accuracy". In: Brain Structure and Function 223, pp. 701–712.

Caminiti, Roberto et al. (2010). "Understanding the parietal lobe syndrome from a neurophysiological and evolutionary perspective". In: European Journal of Neuroscience 31.12, pp. 2320–2340.

Fornito, Alexander et al. (2004). "Individual differences in anterior cingulate/paracingulate morphology are related to executive functions in healthy males". In: Cerebral cortex 14.4, pp. 424–431.

Golesorkhi, Mehrshad et al. (2022). "From temporal to spatial topography: hierarchy of neural dynamics in higher-and lower-order networks shapes their complexity". In: Cerebral Cortex

32.24, pp. 5637–5653.

Gordon, Evan M et al. (2023). “A somato-cognitive action network alternates with effector regions in motor cortex”. In: *Nature*, pp. 1–9.

Ito, Takuya, Luke J Hearne, and Michael W Cole (2020). “A cortical hierarchy of localized and distributed processes revealed via dissociation of task activations, connectivity changes, and intrinsic timescales”. In: *NeuroImage* 221, p. 117141.

Ji, Jie Lisa et al. (2019). “Mapping the human brain’s cortical-subcortical functional network organization”. In: *Neuroimage* 185, pp. 35–57.

Llinás, Rodolfo R (2002). *I of the vortex: From neurons to self*. MIT press.

Mantini, Dante et al. (2011). “Default mode f brain function in monkeys”. In: *Journal of Neuroscience* 31.36, pp. 12954–12962.

Parvizi, Josef et al. (2006). “Neural connections of the posteromedial cortex in the macaque”. In: *Proceedings of the National Academy of Sciences* 103.5, pp. 1563–1568.

Vincent, Justin L et al. (2007). “Intrinsic functional architecture in the anaesthetized monkey brain”. In: *Nature* 447.7140, pp. 83–86.

Whittle, Sarah et al. (2009). “Variations in cortical folding patterns are related to individual differences in temperament”. In: *Psychiatry Research: Neuroimaging* 172.1, pp. 68–74.

Yang, Shimin et al. (2019). “Temporal variability of cortical gyral-sulcal resting state functional activity correlates with fluid intelligence”. In: *Frontiers in neural circuits* 13, p. 36.

Zhang, Songyao, Poorya Chavoshnejad, et al. (2022). “Gyral peaks: Novel gyral landmarks in developing macaque brains”. In: *Human Brain Mapping* 43.15, pp. 4540–4555.

Zhang, Songyao, Tuo Zhang, et al. (2023). “Gyral peaks and patterns in human brains”. In: *Cerebral Cortex*.